THE ASTROPHYSICAL JOURNAL, 409:635–662, 1993 June 1

STAR COUNTS REDIVIVUS. I. A NEW LOOK AT THE GALAXY AT FAINT MAGNITUDES

NEILL REID
California Institute of Technology, Caltech 105-24, Pasadena, CA 91125
AND
S. R. MAJEWSKI[1,2]
Observatories of the Carnegie Institution of Washington, 813 Santa Barbara Street, Pasadena, CA 91101
Received 1992 May 5; accepted 1992 October 23

ABSTRACT

We have used models of the Galactic stellar distribution to analyze Majewski's (1992) deep star-count data toward the north Galactic pole. While the total number counts are in reasonable agreement with the predictions of the current standard models, we find striking discrepancies between the observed and predicted color distributions at faint ($V > 20$) magnitudes: the previously defined "standard" model predicts too many halo stars and too few disk stars. Indeed, our observations show that *disk* stars are the majority population to at least $V = 21$. We have investigated the possible sources of these discrepancies using star-count models and present an interim model which better fits the available data. We find the halo luminosity funcion in the "standard model" is a poor match to globular cluster data. We obtain better agreement with the blue star counts if we adopt an averaged globular cluster function to $M_v = +6.25$ and the nearby-star luminosity function at fainter magnitudes, rather than matching the two functions at $M_v \sim +5$, together with a local number density normalization of $0.15\% \pm 0.03\%$ that of the disk and an axial ratio c/a of 0.8 ± 0.05. For the disk, we find that our data favor a relatively high scale height (1400–1600 pc) and moderate local density (2.5%–2.0% of the disk) for the extended/thick disk component. We also find better agreement with the observed color distributions if the component has a color-magnitude diagram intermediate between the old disk ([Fe/H] ~ -0.1) and 47 Tucanae ([Fe/H] ~ -0.65). The substantial number of stars at $(B-V) \sim 1.5$ that are fainter than $V = 19$ appears to require either higher local densities at $M_v > +10$ or a scale height of $\sim$400 pc for M dwarfs in the old disk.

Subject headings: Galaxy: halo — Galaxy: structure — stars: statistics

1. INTRODUCTION

Star counts have been used to probe the structure of the Milky Way galaxy since the star "gaging" undertaken by William Herschel with his 20 foot telescope (Herschel 1785). The initial studies were, of necessity, simplistic—in the absence of parallax data, Herschel assumed all stars to be of equal candlepower—but, with increased computational power, techniques of growing complexity have been applied to this problem, culminating in the star-count models developed at the beginning of the last decade (notably those of Bahcall & Soneira 1980, hereafter BS80; Bahcall & Soneira 1984, hereafter BS84; and Gilmore 1981, 1984). The availability of large-scale photographic catalogs from automated plate-scanning machines (particularly the data of Kron 1980) and the impending launch of the *Hubble Space Telescope* served as external stimuli for these investigations.

While the initial results of these studies were controversial in certain respects—notably, concerning the necessity for an extended "thick disk" population (Gilmore & Reid 1983, hereafter GR83; Bahcall 1986)—an apparent broad consensus, summarized by Gilmore, Wyse, & Kuijken (1989) and Casertano, Ratnatunga, & Bahcall (1990), now appears to have been reached concerning the structure of our Galaxy, although the status of individual components remains contentious. We find, however, that there are a number of discrepancies between the star counts predicted by these models and the actual observations. It is the intention of this paper to highlight these discrepancies and to suggest modifications that reconcile the models with the observed star counts.

Despite the considerable interest in star counts over the past decade or more, relatively few sets of actual star-count data have been published. Moreover, most of the data which have appeared are based on Schmidt plates (e.g., the Basel surveys summarized by Buser & Kaeser 1985, UK Schmidt data [GR83; Gilmore, Reid, & Hewett 1985], and Kiso Schmidt plates of the north Galactic pole [Stobie & Ishida 1987]) and thus extend scarcely fainter than 19th magnitude. As a result, these data sets are not well suited to probing the structure of the Galactic halo. Recently, however, Majewski (1992, hereafter SRM) has completed an extensive reanalysis of Kron's (1980) plate material covering 0.29 square degrees of Selected Area 57. With access to substantially more plates and with a more accurate, fainter, CCD-based calibration sequence, this work provides not only significantly improved stellar photometry and accurate astrometry to $V \sim 21.5$, but also a stellar sample effectively uncontaminated by extragalactic objects. These are currently the *only* such data which extend fainter than $V = 20$ (Kron's 1980 data in SA68 extend to equally faint magnitudes but have been subject to a less rigorous culling of extragalactic contaminants) and, as we shall show, are as a result the only available data set that allows us to use the halo subdwarfs *in situ* to probe the structure of the halo at large distances from the Galactic plane.

We have matched the SA 57 data against star-count models and find that there are significant discrepancies. In this paper

[1] Visiting Astronomer at Kitt Peak National Observatory, which is operated by the Association of Universities for Research in Astronomy, Inc., under contract with the National Science Foundation.
[2] Hubble Fellow.

we present the results of our initial investigation. Future papers will aim to refine the parameters of our model using new data. The outline of the paper is as follows: § 2 summarizes the properties of the SA 57 data used in this analysis; § 3 reviews previous studies of the relevant Galactic structural parameters and, after a brief description of the characteristics of our model, compares the predictions of a "standard" Galaxy model (which is derived from the results of similar previous analyses) with the SA 57 data. The discrepancies between the "standard" model and the data are discussed in detail in § 4, and in the following section we suggest possible means of reconciling the model with the observations. We would emphasize, however, that with data for only one field, in most cases we cannot draw definitive conclusions concerning individual parameters. Nonetheless, our results demonstrate clearly that none of the published Galactic models prove a good match to the deep SA 57 data.

2. FAINT STELLAR PHOTOMETRY IN SA 57

2.1. *The Observations*

Full details of the deep star-count data can be found in SRM. However, we shall summarize the main properties of the sample here. The faint star counts and colors are derived from stellar photometry on PDS scans of KPNO 4 m plates. All stellar images have been reduced with Stetson's (1979) profile-fitting photometry routine, with measures of the same stars from different plates brought to a common system with plate-to-plate transformations that include both color and positional terms. Once in the common system, the instrumental photometric magnitudes were averaged. A total of 20 plates contributed to the determination of the B_J magnitudes, and 11 plates contributed to the R_F magnitudes. The effective limit of these data is $R_F \sim 21.5$ and $B_J \sim 22.5$. A total of 72 photoelectrically observed stars were used to calibrate the instrumental magnitudes. These calibration stars spanned the entire magnitude range of the data, and were taken from a variety of sources as described in SRM. The random photometric errors are less than ~ 0.02 at $B_J = 22$ and less than ~ 0.03 at $R_F = 21$.

The star/galaxy separation for these data was taken directly from the catalog of Kron (1980). This catalog has been the foundation of a number of surveys regarding stars, galaxies, and QSOs in the last decade, and the object classification has proved robust to the magnitude limits of interest here. Full details on cross checks between the object catalogs are to be found in SRM. The only previous use of the color distributions provided by Kron's catalog in star-count analysis has been in BS80 and BS84 and in Gilmore (1984) [and note that each of the color distributions there presented spans a range of more than 2 mag in $(B_J + R_F)/2$]. Our catalog is improved over that of Kron in several ways. The new photometry makes use of substantially more plate material which has been measured with profile-fitting photometry and which has been photometrically calibrated with more standard stars, particularly at the faint end. In addition, the calibration extends to magnitudes brighter than the plate saturation limit of $B_J \sim 19$ and $R_F \sim 18$. Finally, a substantial amount of progress has been made in understanding the QSO population in SA 57 (cf. Kron et al. 1991), the results of which have been incorporated in our analysis. Note that Kron's catalog still probes fainter than that of SRM and, while we have not used Kron's data in our determination of any Galactic properties, we have included his star counts deeper than $R_F = 21.5$ for qualitative demonstration in several of our figures.

2.2. *On Extragalactic Contamination of Star-Count Data*

The impact of star catalog contamination by extragalactic objects becomes critical when working at magnitudes fainter than $R_F \sim 20$. In Figure 1 we show the differential counts as a function of R_F magnitude for various faint sources in the same 0.29 deg^2 SA 57 field. The star counts from SRM are shown with a solid line. For comparison, the dotted line shows the galaxy counts from Kron (1980). At faint magnitudes ($R_F > 20.5$), the galaxies outnumber stars by about 5:1. This underscores the importance of accurate star/galaxy separation at faint magnitudes: even misclassifying only 10% of the galaxy population as stars can grossly misrepresent the faint star counts. The dashed line represents the contribution of two additional populations which contaminate catalogs of apparent point sources: QSOs and compact, narrow emission line galaxies (CNELGs) at redshifts of $0.1 \leq z \leq 0.7$. The data were taken from the list of such objects with confirmed redshifts from the ongoing QSO survey by Kron et al. (1991). The CNELGs make up about 25% of these extragalatic point sources, which were chosen as QSO candidates based on their nonstellar UBV colors.

According to the top panel of Figure 1, the contamination of the net *number counts* by these extragalactic objects is apparently small, only 5%–10% of the total number of stars for $18 < R_F < 21.5$. However, the impact of these extragalactic contaminants on the faint stellar *color* distributions is more than minimal. This is demonstrated in the lower two panels of Figure 1, where we show the counts of blue objects with $B_J - R_F < 1.17$ (approximately $B - V < 1.0$) and with $B_J - R_F < 0.7$ (approximately $B - V < 0.6$). The QSO + CNELG contamination is most significant for the bluest stars, where, for $20.5 < R_F < 21.5$, the ratio "star:(QSO + CNELG)" is 101:23 for objects with $B - V < 1.0$ and 39:13 for objects with $B - V < 0.6$. *Thus, at least 25% of faint* ($V > 20.5$) *blue* [$(B - V) < 0.6$] *stellar objects are extragalactic at the Galactic pole.*

Even though the Kron et al. (1991) catalog represents the most complete QSO survey at these magnitudes, the actual QSO contamination may, in fact, be even more substantial than just described. Until now we have discussed only spectroscopically confirmed QSOs and CNELGs; a number of candidates with $R_F \geq 21$ still lack adequate spectra for confirmation and remain in the star catalog. Second, recent studies in SA 57 (Majewski et al. 1991; Trevese et al. 1993) of point sources which demonstrate variability but lack detectable proper motions have revealed a population of QSOs which previously were undiscovered because their UBV colors were *similar* to those of Galactic stars. A number of such QSO candidates in our star catalog remain to be confirmed. In Figure 1 we have shown (*dot-dash lines*) how both the (QSO + CNELG) and star counts are affected if these additional QSO candidates are bona fide extragalactic objects and not stars (note that to date four of these objects have been observed spectroscopically by Majewski et al. 1991, with the result that three were found to be QSOs and one a CNELG). In the faintest magnitude bin for which SRM has reliable photometry, $20.5 < R_F < 21.5$, the ratio of stars to (QSOs + CNELGs) may be as low as 91:33 for $B - V < 1.0$ and 35:17 for $B - V < 0.6$.

In summary, we cannot overstress the importance of accurate star/galaxy/QSO separation in surveys which attempt to

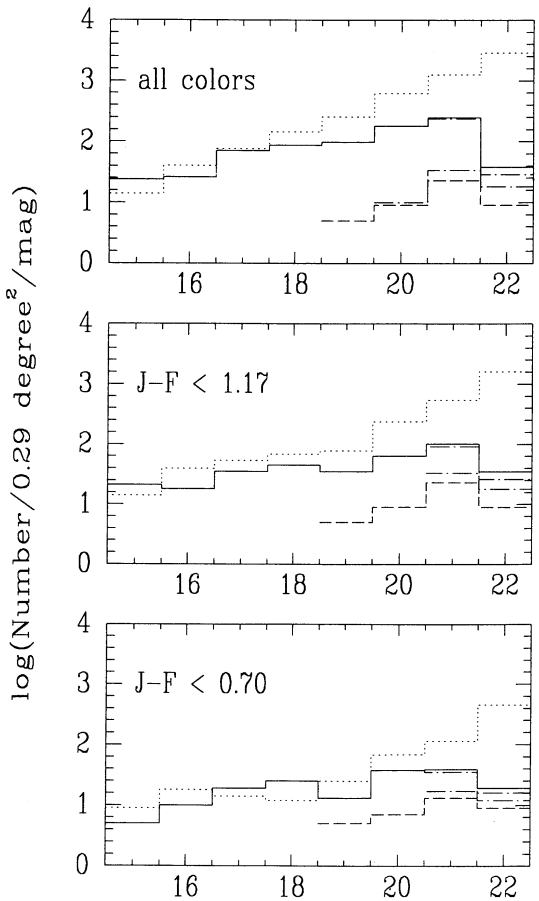

FIG. 1.—Extragalactic contamination in the SA 57 sample. The top panel plots the differential number counts as a function of R_F magnitude for objects in SA 57. The counts for stars (from SRM) are plotted as a solid line; for galaxies (from Kron 1980), as a dotted line; the contributions due to *confirmed* QSOs and compact galaxies (from Kron et al. 1991) are plotted as dashed lines; and the dot-dash lines show the effect of switching the probable QSOs from Majewski et al. (1991) and Trevese et al. (1993) from the star catalog to the QSO catalog. The lower panels show the same distributions, but for colors of $(B_J - R_F) < 1.17$ and $(B_J - R_F) < 0.70$. Note the substantially larger impact of extragalactic contamination on the bluer sample.

study the Galaxy at faint ($V > 20$) magnitudes. There are two major effects at work here: (1) The areal density of stars is declining relative to that of normal field galaxies, so that by $V = 20$ the stars are swamped in number at high Galactic latitudes.[3] (2) The density of QSOs and compact emission-line galaxies which, without spectroscopic confirmation, can easily be confused with stars is rising relative to the density of stars, and can boost the apparent number of blue stars by 30%–50% if not properly accounted for. Unless care is taken to remove these compact extragalactic contaminants, the density of distant Galactic halo stars will be overestimated.

[3] The problem of galaxy contamination is not *limited* to catalogs of very faint stars but arises near the magnitude limit of all surveys. With the benefit of our deep plate material, we have been able to check the reliability of the star/galaxy/QSO separation in three shallower catalogs which overlap our 0.29 deg² area. Of Chiu's (1980) 188 "stars" in 0.1 deg² to $V = 21.3$, five are galaxies and nine are QSOs. The Basel SA 57 survey (Becker & Fenkart 1976) to $V \sim 19$ lists 207 stellar objects in the area we have surveyed, but 16 are galaxies. The Hale 200 inch (5.1 m) SA 57 survey by the Basel group (Becker et al. 1983) is most similar to ours in magnitude limit. It lists 107 stellar objects to $V \sim 21.5$; of these , we find that five are galaxies, seven are QSOs, and two are CNELGs.

3. THE MODEL

3.1. *The Structure of the Model*

All star-count models are based on numerical integrations of the stellar distribution equation devised by von Seeliger (1898),

$$A(m, S) = \sum A_i(m, S) = \Omega \sum \int \Phi_i(M, S) D_i(r) r^2 \, dr \, ,$$

where $A(m, S)$ is the total number of stars of given spectral type (or color index) at given apparent magnitude m the sum of the individual contributions of i populations or subpopulations, $\Phi_i(M, S)$ is the luminosity function of the ith subgroup; and $D_i(r)$ is the density law. To date, most models have chosen to generate analog results—generally tables of the predicted color distribution as a function of position (Galactic latitude and longitude) and apparent magnitude. The current model (which is described in detail by Reid 1992) takes a different tack, generating a catalog of "stars" for a particular (l, b), each with given M_v, distance, colors, and kinematics. (The model constructed by Robin & Crézé [1986a, b] can be used in a similar fashion.) This allows more flexibility in modeling color-magnitude distributions, a more convenient comparison between predicted and observed color-magnitude diagrams, and a ready means of assessing the effects of systematic biases. (Thee last techniques have already been employed in studying the effect of unresolved binaries on photometric parallax analyses; Reid 1991.)

The techniques we adopt are straightforward. Our model essentially starts from the color-magnitude diagram (CMD) chosen for a given subpopulation. We identify a series of nodes (M_v, color) along the CMD and specify the number density (in stars pc^{-3}) between these points (the luminosity function); this method allows us to use unequal magnitude intervals to take account of features such as the subgiant branch, red clump, or horizontal branch. Moreover, we can combine a series of subpopulations with different CMDs (with the appropriate density scaling) to allow for the age distribution or abundance variations within a population.

Dividing the conical sampling volume into segments by distance, we calculate the total number of stars, n, or absolute magnitude $M_v + \Delta M_v$ within each segment, allowing for any decrease due to the adopted density law. (The distance segments are small compared with the slope of the density law, and fractions of stars are carried over into the immediately adjacent, more distant segment.) Each star has an associated absolute magnitude, selected at random from within the interval $\pm\Delta M_v$ [which corresponds to a color range $\pm\Delta(B-V)$ or $\pm\Delta(V-I)$]; the colors appropriate to that M_v, i.e., if the assigned absolute magnitude is

$$M'_v = \langle M_v \rangle + 0.3\Delta M_v,$$

then

$$(V-I)' = \langle (V-I) \rangle + 0.3\Delta(V-I) \, ,$$

and so forth; and a specified distance, r. (Interstellar absorption, A_v, as a function of distance can also be included; we have taken this to be negligible toward the Galactic caps [Burstein & Heiles 1982]). The distances are distributed uniformly in r^3 (to allow for the volume sampling). Finally, the observed magnitude and colors are perturbed by Gaussian distributions to

allow for cosmic scatter in the color-magnitude relations and the observational uncertainties. We have tested our model both against the Bahcall & Soneira export model and against Gilmore's (1984) model and find that, starting with the same input parameters, we reproduce their results.

Our representation of the "standard" Galactic model involves several stellar components or populations which we characterize as being disklike or halo-like.[4] The properties that we adopt for these components are based on previous Galactic structure studies, which we review in the following sections.

3.2. *Disklike Components*

3.2.1. *The Old Disk*

The majority of stars within the solar neighborhood are members of the rapidly rotating Galactic disk population, and their luminosity function is well determined to at least $M_v \sim +13$ through analysis of the nearby ($r < 25$ pc) stars by Wielen, Jahreiss, & Kruger (1983). At fainter magnitudes the form of the luminosity function is less well defined: while the nearby stars suggest a relatively flat luminosity function (with substantial uncertainties given the small-number statistics), deep photometric surveys (Reid & Gilmore 1982; Tinney, Mould, & Reid 1992) indicate that the luminosity function peaks at $M_v \sim 12.5$. It has been suggested that the differences between the local and photometric-parallax–defined luminosity functions may stem from the presence of unrecognized binaries in the latter (Kroupa, Tout, & Gilmore 1991), but Reid (1991) has shown that binarism has relatively little effect on the *shape* of the luminosity function. In any event, as we discuss in § 3.2.3, these faint disk stars are of significance only at magnitudes fainter than $V \sim 21$.

The nearby stars also provide the color-magnitude relations for the disk. Bessell (1990) has obtained *BVRI* observations of more than 900 stars from the Gliese (1969) catalog, while Leggett (1992) includes infrared (*JHKL*) data in her compilation of multicolor photometry. Our color-magnitude relations are based on Bessell's *BVRI* data, but since the main differences between these data and Leggett's compilation are among the reddest stars, adopting Leggett's system leads to no significant changes. We have used NGC 188 (McClure & Twarog 1977) as the template for the giant branch (although we should note that giants have negligible impact on the polar star counts fainter than $V \sim 14$).

It is well known that the velocity dispersion perpendicular to the Galactic plane, σ_z, increases rapidly with age (see, e.g., Wielen's 1974 analysis of the McCormick dwarfs), and, as a result, the youngest stars and gas have a distribution that is more confined to the plane than the contemporaries and antecedents of the Sun. Star-count models (BS84; Gilmore 1984; Yoshii, Ishida, & Stobie 1987; Robin & Crézé 1986a) generally take account of this by adopting exponential density laws[5] with scale heights ranging from 100 pc for the most luminous ($M_v \leq \sim +2$) stars to 350 pc or more for the lower luminosity ($M_v > +4$) stars. The observations upon which these results are based are summarized in GR83; note that there is no direct measurement of the scale height of stars with $M_v > +10$. Recently, however, Kuijken & Gilmore (1989) have derived a scale height of 249 pc from a sample of K dwarf stars [$0.85 \leq (B-V) \leq 1.20$] used in their study of the gravitational force law, K_z. The distances were derived using photometric parallaxes [M_v, $(B-V)$] and the scale heights of both old disk and extended/thick disk (1000 pc) are smaller than the $(V-I)$-based values for the same stars (§ 4.2). We shall show that models with such small scale heights are inconsistent with the observed star counts.

3.2.2. *The Extended/Thick Disk*

Most studies of the density distribution perpendicular to the disk have derived density distributions which show a significant change in slope at heights of 1–2 kpc above the plane (for example, Elvius 1965; Becker & Fenkart 1976). However, Gilmore & Reid (1983) were the first to draw particular attention of this phenomenon. In their analysis of the density distribution toward the south Galactic cap, they suggested that the "extra" stars (over a thin-disk 325 pc exponential distribution) at heights of 1 kpc or more represented a separated stellar population, the "thick" disk, possibly related to the intermediate Population II stars discussed at the Vatican conference (Oort 1958). The main impetus for the latter suggestion was the fact that the exponential distributions fitted to the thick disk had scale heights of $\sim$1450 pc, implying velocity dispersions of $\sigma_w \sim 60$ km s^{-1}, similar to those of the local metal-rich RR Lyrae stars (Woolley 1978; Strugnell, Reid, & Murray 1987). These variables have a substantial mean rotational lag ($\sim$100 km s^{-1}) with respect to the Sun, suggestive of an origin different from that of the rapidly rotating old disk—hence the hypothesis of the thick disk as a separate, intermediate population. GR83 also pointed out that the steepening of the bright end of the luminosity function with height above the plane indicated that the thick disk was an old (several Gyr) population, and they estimated the local density normalization as $\sim$2% that of the disk. Gilmore et al. (1985) found that star counts to $V \sim 19$ toward ($l = 37°$, $b = -51°$) were consistent with these parameters.

[4] We should make clear that by "halo" we mean the old *stellar* populations of the Galaxy; we avoid the term "spheroid," which has been used on recent occasions with reference to the halo, to the Galactic Bulge, and, occasionally, to the dark matter distribution. (Confusingly, the last is also referred to variously as the corona, the "dark halo," or simply the "halo.") For the remaining subpopulations we have followed the form, if not the exact terminology, of the Vatican Stellar Population Conference (Oort 1958); hence we have a young disk ('extreme Population I" in Oort 1958), an intermediate disk ("older Population I"), and an old disk ("old disk"), while the halo is equivalent to the "extreme Population II." Finally, the extended/thick disk, consisting of stars with spatial and kinematic properties intermediate between old disk and halo, has some morphological characteristics similar to the "intermediate Population II" of the Vatican conference.

[5] The origin of the use of a *single* exponential distribution to characterize both young and old disk populations probably lies in Kapteyn's (1922) demonstration (later expanded by Oort 1932) that a population having a Gaussian velocity dispersion will describe an exponential density law in a plane-parallel disk. (Note that the plane-parallel approximation breaks down when stars reach sufficient height above the midplane that they "see" the concentration of mass toward the Galactic center.) Camm (1950) discusses other solutions to this problem, including the sech^2 distribution (which tends toward an exponential at large radii) used by van der Kruit & Searle (1982) in their studies of edge-on spirals. It is only recently that the single-exponential approximation has been assumed sufficient for the disk as a whole; Elvius (1965) avoids giving an explicit form for the density law, while other earlier measurements use other functional forms. For example, in Schmidt's (1959, 1962) investigation of the distribution of G, K, and early M dwarfs, the results, which are often misquoted as being exponential scale heights, are in fact "equivalent widths"—the ratio between the surface density and the volume density. However, despite these caveats as to past usage, combinations of exponential functions remain a useful approximation to the density distribution of the disk. But although we use exponentials to characterize the overall density distribution, we would emphasize that these are no more than convenient fitting functions, and we shall resist the temptation to ascribe physical significance to the individual components.

Since the identification of the "thick disk," there have been a number of investigations aimed at setting more accurate constraints on the density distribution. (There is also a continuing debate as to whether these stars constitute a separate population [Gilmore & Wyse 1985; Gilmore et al. 1989; Carney, Latham, & Laird 1989] or simply the high velocity dispersion tail of the old disk [Norris 1987a; Norris & Green 1989; Norris & Ryan 1991]. We discuss this further below.) In Table 1 we summarize the density parameters of the extended/thick (E/T) disk from a variety of sources. Table 1A contains references which have used specific E/T disk parameters explicitly in self-consistent, global Galactic models; that is, these analyses present models which parameterize all stellar populations and aim at accurate prediction of the full stellar number-magnitude-color distribution. These studies have derived the scale heights and normalizations either directly from fitting star-count and/or color data (Gilmore 1984; Robin & Crézé 1986a; Yoshii et al. 1987; Yamagata & Yoshii 1992), or in the case of del Rio & Fenkart (1987), through favorable direct comparison of a given set of parameters to star-count data.

We make a distinction between these *global* investigations and other studies which have identified a specific set of objects as tracers of the thick or extended disk (Table 1B). Thus, Gilmore & Wyse (1985), Sandage & Fouts (1987), Sandage (1987), and Casertano et al. (1990) derive their results from kinematically selected samples of stars taken to be representative of the thick disk; Friel (1987) and Morrison, Flynn, & Freeman (1990) use giant stars; Rose (1985) uses a sample of red horizontal-branch stars (although Norris 1987b and Norris & Green 1989 suggest that the bulk of the stars are from the giant-branch red clump found in old disk clusters), and Layden's (1992) results are based on observations of metal-rich RR Lyrae stars. We have also included in Table 1B those analyses which are based on photometric parallax analysis of normal field stars (GR83; Koo, Kron, & Cudworth 1986;

TABLE 1A

DISK PARAMETERS DERIVED FROM STAR-COUNT MODELS

Model	z_0(old disk) (pc)	z_0(E/T disk) (pc)	ρ_0(E/T disk) Relative to Old Disk (%)
Gilmore 1984	325	1300	2
Bahcall & Soneira 1984	325	...	...
Robin & Crézé 1986b	200–475	1200–2200	1.6
del Rio & Fenkart 1987	300	1000	2
Yoshii et al. 1987	325	950	2.24
Yamagata & Yoshii 1992	350	900	1.9
Standard model	325	1200	2

NOTE.—The scale heights determined for the old and E/T disk and the normalization of the latter component (in number density relative to the old disk) in the star-count analyses published by Gilmore 1984, Bahcall & Soneira 1984 (no E/T population), del Rio & Fenkart 1987, Yoshii, Ishida, & Stobie 1987, Yamagata & Yoshii 1992 and Robin & Crézé 1986b. In the last model, both the old disk and E/T disk scale heights are allowed to vary as a function of age (M_v). The final line lists the parameters we have have adopted for our standard model.

TABLE 1B

THE EXTENDED/THICK DISK

Reference	Method	z_0 (pc)	ρ_0 Relative to Old Disk (%)
Gilmore & Reid 1983	Field [M_v, $(V-I)$]	1450	2
Gilmore & Wyse 1985	σ_w, [Fe/H]	1000–2000	2
Rose 1985	Field red horizontal branch stars	500–1000	~10
Koo et al. 1986	1500	2	...
Sandage & Fouts 1987	Nearby high-μ stars	~1000	>2
Friel 1987	Field giants	<1000	~5
Sandage 1987	σ_w	940[a]	11
Norris 1987a[b]	σ_w, [Fe/H]	1100	3.4
Kuijken & Gilmore 1989	[M_v, $(B-V)$]	1000	4
Casertano et al. 1990	Nearby high-μ stars	<1000	10 ± 5
Layden 1992	RR Lyrae stars	700 ± 300	...
Morrison 1992	Metal-poor E/T stars	~2000	...
von Hippel & Bothun 1992[c]	*uvby* of field stars	860 ± 90	...

[a] Sandage's 1987 analysis does not predict exponential density laws. The scale height listed is the height at which the density has declined by a factor of $1/e$ from that at $z = 0$.

[b] In the extended disk mode, Norris 1987a argues that the "thick disk" represents the higher velocity stars in the old disk. The parameters listed are for the least abundant ([Fe/H] = −0.56) of his four-component model. In this approximation to a continuous distribution, Norris also places 5.4% in a [Fe/H] = −0.46, 450 pc scale height distribution. Both scale heights follow from assuming a 230 pc scale height for the dominant fraction of the old disk.

[c] Systematic errors in the [Fe/H] calibration may raise the scale height estimate to 950 ± 90 pc.

Kuijken & Gilmore 1989; von Hippel & Bothun 1992) but which do not test the results for full consistency; that is, no star-count models are constructed to test the predictions against the complete color-magnitude distributions of all Galactic components.

Broadly speaking, most of the investigations cited in Table 1B arrive at scale heights that are lower than the original result in GR83 (and in most of the models in Table 1A), while the local normalizations in Table 1B are typically higher than those in Table 1A. In general, these two parameters are anti-correlated when fitted simultaneously. Note also that the more recently quoted scale heights for the E/T disk are generally lower than the earlier determinations. We have adopted the same scale length (3.5 kpc) for both the old disk and the E/T disk, but, since we consider here only the polar star counts, this parameter has no effect on the model predictions.

Although Morrison et al.'s (1990) observations suggest that the metallicity distribution of the E/T disk may extend to [Fe/H] ~ -1.5, the mean abundance that is typically quoted is [Fe/H] ~ -0.6 (Gilmore et al. 1989; Carney et al. 1989). Moreover, these stars have been linked with the metal-rich "thick-disk" globular clusters (Zinn 1985; Armandroff 1989). Motivated by these results, and by the findings of Rose & Agostino (1991) and Friel (1988), we have used the metal-rich ([Fe/H] ~ -0.65) globular 47 Tucanae as the template for the color-magnitude diagram for this subpopulation in our "standard" model. The $(B-V)$ colors are taken from Hesser et al.'s (1987) observations and the RI data from the VandenBerg & Bell (1985) models. This cluster is slightly more metal-poor than the accepted mean abundance of the E/T disk, but the VandenBerg & Bell (1985) tracks indicate that an offset of 0.02 mag in $(B-V)$ is all that is required to match [Fe/H] $= -0.5$ at the turnoff (Carney et al. 1989).

One could argue with our choice of template, since metal-rich RR Lyrae stars, often considered to be tracers of the "thick disk," are notable in 47 Tuc by their scarcity. In justification, we point out that these models are indicative rather than definitive, and are not aimed at testing the horizontal-branch structure of the halo; that the 47 Tuc main sequence is the best studied among metal-rich globulars; that the two other well-studied metal-rich clusters which have RR Lyrae stars, M71 and NGC 6171, both have high foreground reddening (E_{B-V} of 0.31 [Arp & Hartwick 1971] and 0.38 mag [Da Costa, Mould, & Ortolani 1984], respectively, as opposed to 0.04 mag for 47 Tuc), rendering them less suitable as templates for color-magnitude diagrams; and, finally, that more recent estimates of the "thick-disk" kinematics are, as we discuss further below, in less accord with those of the metal-rich RR Lyrae stars, which may themselves not be representative of a single population or subgroup.

Finally, a comment on the naming of things: the original characterization of the thick disk as a separate population stems from the analogy drawn between the extra stars in GR83 and the metal-rich RR Lyrae stars; based on the 1500 pc scale height fitted to the thick disk, GR83 inferred a velocity dispersion of $\sigma_w \sim 60$ km s^{-1} and, taking the RR Lyrae stars as tracers, a rotational lag of ~ 100 km s^{-1} (Strugnell et al. 1987). Subsequent observations have shown that the rotational lag (relative to the Sun) of these stars is no more than ~ 35–40 km s^{-1} (Dawson 1986; Morrison et al. 1990; Casertano et al. 1990), although there are observations (Murray 1986; Spaenhaver 1989; SRM) which suggest that the asymmetric drift increases with height above the Galactic plane. However, the term "thick disk" continues to be associated with a separate stellar population (Carney et al. 1989; Wyse & Gilmore 1989), distinct from both old disk and halo. Carney et al., in particular, have argued that the abundance distribution of the "thick disk" defined from their observations of proper-motion stars is distinct from that of the old disk, and indicative of their being a separate population.

On the other hand, Norris (1986, 1987a, b) has argued that the complex density distribution perpendicular to the Galactic plane reflects the fact that the disk incorporates stars with a range of ages with different velocity dispersions, and hence vertical density laws. The highest velocity dispersion component in the Norris (1987a) four-component model has $\sigma_w = 33$ km s^{-1}—somewhat less than the ~ 40 km s^{-1} measured at large distances above the plane. Note, however, that Wielen & Fuchs (1983) have shown that velocity dispersions of 40–50 km s^{-1} can be achieved if there is sufficient infall over the history of the Galactic disk. In any case, the large-scale-height, "extended disk" population comprises the oldest stars in the disk, which have been subject to the most scattering out of the Galactic plane. Norris & Ryan (1991) have argued that this model gives a better representation of the abundance distribution observed in proper-motion selected samples.

Both the terms "thick disk" and "extended disk" thus carry the undesirable baggage of associations with specific models of formation, as does the expression "intermediate Population II" used in the Vatican conference (Oort 1958). We prefer to deal with the data without regard to the possible origins of the density distribution—whether separate episodes of star formation, scattering by massive objects over the lifetime of the disk, or the response of the early disk to mergers—and will therefore engage in fence-sitting by referring to these stars as the E/T disk.

3.2.3. *Parameters for the "Standard" Model*

Our aim in constructing a standard model of the Galaxy is to test how well recent Galactic models match the new, faint data in SA 57. Table 1A lists the parameters used to characterize the old disk and the E/T disk in the most recent star-count models, and the final line lists the values that we have chosen as appropriate to characterize the average properties of these models. While other values for various parameters, in both disk and halo, are quoted in the literature (as discussed above), the five models listed in Table 1B are the most recent that actually are derived from (or at least matched against) star-count analyses—that is, they represent self-consistent, global Galactic models rather than determinations of specific, individual parameters.

Of the five models listed, the most complex is the Robin & Crézé (1986a, b) evolutionary model, which allows the scale heights of both disk and E/T disk (intermediate Population II in their model) to evolve with age. Hence, disk stars aged 3 Gyr ($\sigma_w \sim 20.5$ km s^{-1}) have a scale height, z_0, of 360 pc, while 5 Gyr and older stars have $z_0 = 475$ pc ($\sigma_w \sim 25$ km s^{-1}). Similarly, the intermediate Population II has a scale height ranging from 1180 pc (age 12 Gyr) to 2210 pc (14 Gyr). We have adopted a similar approach, although with fewer subdivisions.

The parameters of our "standard" model are generally averages of the results from previous studies. For the traditional thin disk, we have defined three subpopulations: a young disk with an age of $\sim 3 \times 10^8$ yr, a scale height of 100 pc and a Hyades-like color-magnitude diagram (from Upgren, Weis, & Hanson 1985 and references therein); an intermediate-age disk

($\tau \sim 2$ Gyr) with a 250 pc scale height; and an old disk, scale height 325 pc. The color-magnitude diagrams for the latter two components are, as we noted above, based on Bessell's (1990) photometry of nearby stars. Finally, we have adopted a scale height of 1200 pc and a 47 Tuc–like color-magnitude diagram for the E/T disk. We have allowed for observational uncertainties by adding Gaussian errors to the V-magnitude ($\sigma = \pm 0.05$ mag) and to the colors ($\sigma = \pm 0.08$ mag) of each "star" generated by the model. These uncertainties match the Schmidt-based data sets.

Several recent investigations suggest strongly that the Sun is situated above (i.e., toward the north Galactic pole) the midplane of the Galactic disk. Blaauw (1960) estimated the offset as 30 pc based on young disk tracers, and Magnani, Blitz, & Mundy (1985) arrive at a similar offset from molecular cloud observations, Toller (1981) previously derived an offset of 12 ± 2 pc from *Pioneer 10* data, and Djorgovskii & Sosin's (1989) analysis of *IRAS* source counts also leads to a smaller offset of 15–22 pc. Most recently, Yamagata & Yoshii (1992) have used star-count models to analyze north and south Galactic pole observations and derive $\Delta z = 40$ pc. We have adopted a 30 pc offset for our model calculations.

The luminosity functions of the various components are based on combining the nearby-star results of Wielen et al. (1983, hereafter WJK) for $M_v < +11$ with the photometric-parallax–based calculations for fainter stars (Reid 1987), and we have used the lifetimes compiled by Miller & Scalo (1979) (and an assumed age of 10 Gyr for the disk) to divide the stars among the subpopulations. Thus, all stars with $M_v < +2$ are assigned to the young disk, together with 30% of the $M_v = +2$ stars, 20% at $M_v = +3$, 10% at $M_v = +4$ and 3% for $M_v \geq +5$; the remaining stars with $+2 \leq M_v \leq +3$, 45% of the $M_v = +4$ stars, and 17% of all fainter stars are counted among the intermediate disk; and the old disk includes 45% of the observed space density at $M_v = +4$ and 80% of all lower luminosity stars. In the event, neither the young disk nor the intermediate disk proves to make significant contributions to the polar counts. The E/T disk is assumed to have a luminosity function that is similar in shape to that of the old disk but is scaled to 2% of the *total* local number densities.

3.3. *The Halo-like Components*

3.3.1. *Previous Studies of the Halo*

Apart from general star-count analyses, the structure of the Galactic halo has been probed using both nearby samples of high proper motion and/or low-metallicity stars to infer the kinematic properties, and more distant, luminous stars, such as RR Lyrae stars or K giants, as tracers of the *in situ* density distribution. In the first case, since the halo has a low (or perhaps even retrograde) mean rotation and a high velocity dispersion, subdwarfs make a substantial contribution to samples of high proper motion stars, and most estimates of the local halo-to-disk ratio rest on analyses of these catalogs. (We discuss the kinematics of the halo in more detail in § 4.1.2.) In one of the earliest of these studies, Schmidt (1975) applied the $V/V_{\max}$ technique to a sample of 17 stars with high tangential velocities ($V_t > 250$ km s^{-1}, assumed to be the median tangential velocity of halo stars) to derive an estimate 0.125% for the local halo-to-disk ratio (note that this is a *mass* ratio, relative to the total [stars + gas] disk mass, and therefore corresponds to a *number* ratio of ~0.25%). Clearly, Schmidt's estimate is dependent on the kinematics one associates with the halo, and most subsequent studies (Richstone & Graham 1981; Dawson 1986; Bahcall & Casertano 1986) have analyzed the proper-motion data in conjunction with Monte Carlo style simulations of the concomitant selection effects. These subsequent analyses derive number density normalizations, ρ_0, in the range 0.15%–0.35% of the local disk density, with much of the range in the results stemming from the different kinematics adopted for the halo. We shall discuss the influence of these effects in more detail in § 4.1. For the moment we note that studies of local RR Lyrae stars (Suntzeff, Kinman, & Kraft 1991) and field horizontal-branch stars (Preston, Shectman, & Beers 1991) favor densities toward the lower end of this range.

Studies of nearby proper-motion stars have also been used in attempts to derive the luminosity function for the halo, although with the small-number statistics the results are not conclusive. Both Schmidt (1975) and Bahcall & Casertano (1986) concluded that the subdwarf luminosity function is not inconsistent in shape with that of the old disk. (Richer & Fahlman's recent results [Richer & Fahlman 1992] suggest that the halo luminosity function may continue to increase beyond $M_v \sim +12$, in contrast to its behavior in the disk, but such stars have negligible effect on star counts to $V = 22$.) Given that the halo is an old population, with an age corresponding to a main-sequence turnoff of $M_v \sim +4$, star-count models have used the luminosity functions derived for globular cluster stars to define densities of the brighter (evolved) stars and have used the disk luminosity function for the main-sequence stars. The transition between the two functions is usually set in the range $+4 \leq M_v \leq +4.5$ (Gilmore 1984, Fig. 6; Bahcall 1986, Fig. 12).

Since the halo is metal-poor, one must adopt an appropriate color-magnitude diagram in star-count models. Studies of nearby proper-motion stars (Carney et al. 1990b; Ryan & Norris 1991) show that their metallicity distribution is similar to that of the globular clusters, with the median abundance at [Fe/H] ~ -1.6 and a relatively small tail to abundance of -4. RR Lyrae stars show no evidence for a radial abundance gradient *outside* the solar circle, with the mean metallicity being $\langle$[Fe/H]$\rangle = -1.65 \pm 0.3$ at these radii (Suntzeff et al. 1991). SRM derived an average abundance of [Fe/H] $= -1.43$ for the SA 57 stars more distant than 5 kpc. Kraft et al. (1992) have recently shown that a detailed analysis of giants in M3 and in the field halo reveals striking similarities—in particular in the O, Na, and CN abundances—and they suggest that M3 has a similar age and history of enrichment to those of the field stars. Kraft et al. determine a mean abundance of -1.47 ± 0.01 for the M3 giants, close to the abundance estimate for halo field stars (previous abundance estimates by Suntzeff 1981 and Zinn & West 1984 give [Fe/H] $= -1.6$ for the cluster). Finally, Kraft (1989) has pointed out that the relative numbers of blue horizontal-branch stars and red giants in deep surveys (such as those of Reid & Gilmore 1982 and Hartwick 1983) match those expected for a population with a Hess diagram resembling the intermediate abundance clusters M3 and M5.

Other authors have argued that M13, with a bluer horizontal branch, is a better template for the halo. Both Preston et al. (1991) and Green & Morrison (1992) find that the local horizontal branch is blue; the former authors derive a number ratio of ~6.5:1 between blue horizontal-branch stars and RR Lyrae stars. Kinman (1992), on the other hand, finds the ratio to be nearer unity in his fields. We should emphasize here that these questions, while of considerable importance for our understanding of the formation and evolution of the halo, are

of little significance for our star-count work. Our primary concern is in matching the colors at the turnoff; evolved stars make negligible contribution to star counts at the pole at magnitudes fainter than $V = 17$. Constraining the finer details of the color-magnitude diagram demands a much more extensive data set than we have available at present. Hence, any of the intermediate-abundance clusters M3, M5, and M13 are adequate for our present purposes, and we have chosen to use M3.

The halo density distribution has been mapped primarily using globular clusters, RR Lyrae stars, and blue horizontal-branch stars. Harris (1976) and Zinn (1985) have shown that the metal-weak globulars have a distribution consistent with an $r^{-3.5}$ power-law distribution (the metal-rich [Fe/H] < -1 systems are more confined to the Galactic plane; Armandroff 1989). Weighting the cluster distribution by mass using a mean M/L ratio leads to a less steep density variation closer to r^{-3} (Carney et al. 1990a; Suntzeff et al. 1991) (although see the next paragraph for a caveat). RR Lyrae stars can also be used as halo tracers, although abundance gradients might introduce significant systematic selection effects, since the horizontal branch for very metal-poor stars may be too blue to intersect the instability strip. In addition, metal-poor RR Lyrae stars have lower amplitudes and longer periods (Preston 1957) and are therefore more difficult to detect. In the absence of a significant abundance gradient (Suntzeff et al. 1991), however, RR Lyrae stars are excellent density tracers, and indicate a less steep distribution; Saha (1985) finds his data at radii of between 5 and 25 kpc to fit an r^{-3} distribution (with an apparent steepening in the density law at larger radii), while Hawkins (1984) derives $r^{-3.1}$. Kinman (1992) has combined both RR Lyrae stars and field horizontal-branch stars in several fields to derive an average number density gradient of $\rho(r) \propto r^{-3.5}$.

The halo density distribution is defined both by the density law and by the overall flattening (c/a) of the distribution (which is generally assumed axisymmetric about the Galactic rotational axis). If we take the metal-poor globular clusters as indicators of the shape of the halo, then we infer a nearly spherical distribution. However, one should be careful in using the globulars in this context as tracers of the field halo, first, since it is possible that the conditions for forming $10^5\ M_\odot$ mass concentrations of stars were markedly different from those which governed "normal" halo star formation, in which case it is entirely possible for the two distributions to have started with different radial density gradients, and, second, because the inner clusters may have suffered more attrition over Galactic history. Nonetheless, most of the early star-count analyses (Gilmore 1984; BS84) also arrived at axial ratios of $\sim$0.8–0.9, consistent with the Oort & Plaut (1975) RR Lyrae analysis. Yamagata & Yoshi (1992) derive a halo flattening of $c/a = 0.84$ from their analysis of Kron's (1980) star counts in SA 68 and SA 57.

Initial dynamical studies (White 1985; Levison & Richstone 1986) found this value difficult to reconcile with the strongly anisotropic velocity dispersions inferred from local halo tracers such as the metal-poor RR Lyrae stars and the nearby subdwarfs, which appeared to require a higher degree of flattening. More recent studies (Arnold 1990; van der Marel 1991), however, have shown that the theoretical picture is less clear and that the triaxiality of the local velocity ellipsoid need not imply substantial flattening ($c/a < 0.5$) of the halo.

On the other hand, there is some observational evidence for at least a component of the Galactic halo with an axial ratio substantially less than unity. Wyse & Gilmore (1989) have suggested that a comparison of the number of blue stars in two fields at different Galactic latitudes is more consistent with $c/a \lesssim 0.6$ rather than $\sim$0.8 (we return to this in § 4.1), while Wesselink (1987) reanalyzed the Oort/Plaut RR Lyrae data, deriving axial ratios near 0.6. H. Morrison & P. Harding (1992, private communication) find that their observations of K giants toward the Galactic bulge suggest a significant flattening in at least the inner halo, while other observations also imply that the halo density distribution may be complex. Hartwick (1987) found that the distribution of the metal-poor RR Lyrae stars required at least a two-component halo, with approximately 90% of the nearby stars in a flattened component ($c/a \sim 0.5$) and the remainder in a near-spherical distribution. As Preston et al. (1991) have pointed out, evidence for flattening in the inner halo had been discovered previously by Kinman (1965),[6] while Kinman, Wirtanen, & Janes (1966) originally suggested that the halo axial ratio c/a increases as a function of radius (although the metal-poor E/T disk RR Lyrae stars may contaminate these samples). Sommer-Larsen & Zhen (1990, hereafter SLZ) have derived similar results for nearby, metal-poor ([Fe/H] ≤ -1.5) subdwarfs. Integrating the orbits within potentials derived from Sommer-Larsen's (1986) models, they assign $\sim$60% of the local stars to a relatively spherical population ($c/a \sim 0.85$), while the remainder have significantly flatter orbits ($c/a \sim 0.4$). They derive a density distribution $\rho(r) \propto r^{-3.3}$. The models, however, continue to have problems in accommodating fully the low velocity dispersions observed among distant K giants by Ratnatunga & Freeman (1989).

3.3.2. *Parameters for the "Standard" Model*

As with the disk, the halo parameters for our "standard" model are matched against those used in recent star-count models. We have assumed that the halo luminosity function has the same form as that of the disk, truncating the main sequence at $M_v = +4.5$ with the densities at brighter luminosities matched to the average globular cluster function presented by Gilmore (1984). We have adopted a local normalization of 0.15% of the disk density. The color-magnitude diagram for both the main-sequence and evolved (red giant and horizontal-branch) stars is based on the intermediate-abundance globular cluster M3. While most observational studies of the halo describe the density distribution in terms of a power law, the star-count models generally adopt a de Vaucouleurs $r^{1/4}$ spheroid as appropriate, with most taking the effective radius to be 2.7 kpc (de Vaucouleurs 1977). This gives a radial density distribution that is relatively close to an $r^{-3.3}$ power law. For our "standard" model we include a single-component halo with an axial ratio (c/a) of 0.85, consistent, as Table 2 shows, with the values adopted in previous star-count models.

3.4. *A Comparison of the "Standard" Model with the SA 57 Data*

Figure 2*a* shows the observed [V, ($B-V$)] color-magnitude diagram toward the north Galactic pole, derived from SRM's [B_J, ($B_J - F$)] data using the color transformations given in

[6] Preston et al. (1991) comment that they are "surprised by the extent to which [Kinman's] compelling evidence has been ignored in subsequent investigations of halo structure."

TABLE 2

HALO PARAMETERS DERIVED FROM STAR-COUNT MODELS

Model	b/a	Density Law	R_e (pc)	ρ_0 Relative to Old Disk (%)
Gilmore 1984	0.85	de Vaucouleurs	3000	0.125
Bahcall & Soneira 1984	$0.80^{+0.20}_{-0.05}$	de Vaucouleurs	2700	0.2
Robin & Crézé 1986b	0.85	de Vaucouleurs	2700	0.2
		$r^{-3.1}$	...	0.2
del Rio & Fenkart 1987	0.85	de Vaucouleurs	2700	0.1
Yoshii et al. 1987	0.9	de Vaucouleurs	2700	0.1
Yamagata & Yoshii 1992	0.84	de Vaucouleurs	2700	0.11
Standard model	0.85	de Vaucouleurs	2700	0.15

NOTE.—Summary of the parameters adopted for the axial ratio, density law, and local density normalization of the Galactic halo in the more recent Galactic models. Again, the final line lists the parameters adopted as our standard model.

that paper. The error bars show the appropriate random photometric uncertainties. Data for the brighter individual stars are listed by SRM, and we have tabulated the differential star counts—both $[R_F, (B_J - R_F)]$ and $[V, (B-V)]$—in Table 3. We can compare these observations with the predictions of the "standard" model, plotted in Figure 2*b*, which has the familiar bimodal color distribution originally pointed out by Kron (1980). The red peak in this distribution is due to stars in the disk, with more distant halo stars contributing the bluer sequence (Gilmore 1981). Since this is of some importance in understanding the color-magnitude diagrams at faint magnitudes, we briefly review this point.

The distance distribution of stars from a given subpopulation is simply the convolution of the density law of that subpopulation with the volume element (i.e., $\frac{1}{3}\Omega r^3$, where Ω is the solid angle). The different scale heights of the disk, E/T disk, and halo lead to radically different distance distributions, as Figure 3 illustrates. The old disk has a distribution with a median value of ~ 700 pc [or $(m - M) \sim 9 \pm 1.5$], while the halo stars are drawn from a much broader span of distance. Hence, as one samples the disk at fainter *apparent* magnitudes, one is also sampling (on average) fainter *absolute* magnitudes. This is in contrast to the halo star distribution, which even at $V \sim 22$ is dominated by stars from a relatively limited range in

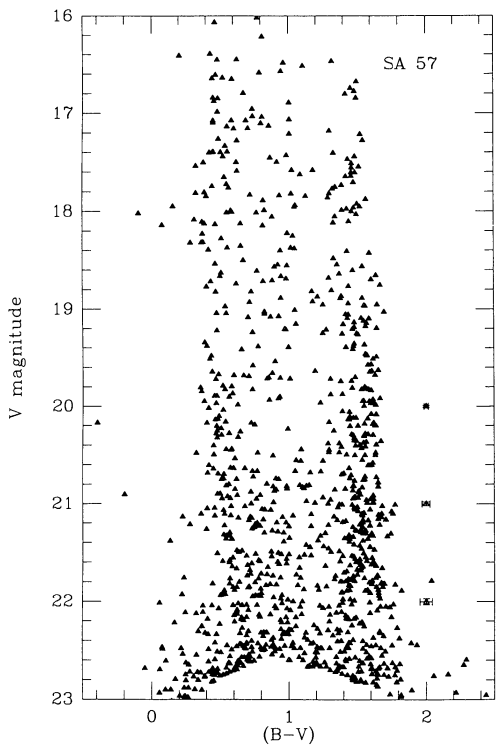

FIG. 2*a*

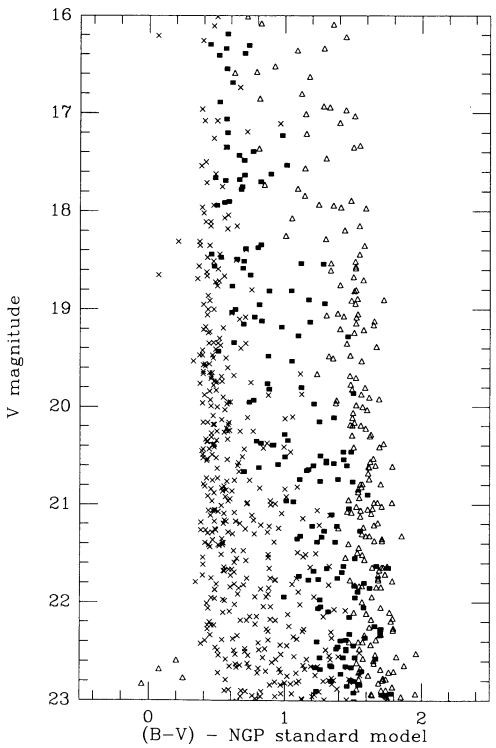

FIG. 2*b*

FIG. 2.—(*a*) Observed $[V, (B-V)]$ color-magnitude diagram toward the north Galactic pole, derived by transforming Majewski's (1992) B_J, R_F photometry of stars in the SA 57 field. The error bars illustrate the uncertainties as a function of magnitude. (*b*) Color-magnitude diagram predicted for SA 57 (0.3 deg^2) by the standard model. The open triangles are old disk stars, the filled squares represent the E/T disk, and the crosses are the halo contribution.

TABLE 3A

SA 57 STAR COUNTS AND B_J, R_F DATA

	$B_J - R_F$												
R_F	0.1	0.3	0.5	0.7	0.9	1.1	1.3	1.5	1.7	1.9	2.1	2.3	2.5
15.10.....			1		3								
15.30.....					1	1			1				
15.50.....				3									
15.70.....				1	2								
15.90.....			1		1			1					
16.10.....						2	1		5				
16.30.....		1	2	1	1								
16.50.....			2	3		1				1			
16.70.....			4		4	2		1	1	1			
16.90.....			2	3	2	1		1	6				
17.10.....			1	4		3	3	1	4	1			
17.30.....			4	3			1	3	6	1			
17.50.....		1	1	3	2	1	3	2	1				
17.70.....		1	2	3	2	1			1	1			
17.90.....	2	1	3	1	1	1	3	1	2	3			
18.10.....	1		3	3		3		1	2	1			
18.30.....		1	2	1	2	4	1	2	3	5	1		
18.50.....			2	2	1	1	2	1	7	5			
18.70.....			2	1	3	2	1	2	7	6			
18.90.....			1	1	2	3				6			
19.10.....			2	1	1	1		2	4	6			
19.30.....			3		1	4	1	1	1	10			
19.50.....			3	3	3	3		1	9	9			
19.70.....			6	4				2	8	10			
19.90.....			4	2	2	1	1	3	4	6			
20.10.....	1		6	5	1	1	3	2	8	7			
20.30.....		1	3	5	3	2	6	1	12	13	4		
20.50.....			4	7	4	5	1	6	8	12	2		
20.70.....			2	6	5	4	3	2	11	12			
20.90.....	1		4	4	11	7	2	5	9	11			1
21.10.....		2	1	9		6	3	2	12	17	3		
21.30.....	1		1	7	9	6	4	4	12	7	4		
21.50.....				5	9	6	3	5	11	6	2		
21.70.....		1	2	8	7	7	4	5	5	6	2	3	
21.90.....	1	2	4	10	8	12	7	6	12	16	8		3

NOTE.—Star counts for the 0.3 deg^2 field of SA 57. The data brighter than $R_F = 21.5$ are drawn from Majewski's 1992 survey, with the fainter data from Kron 1980. Known extragalactic objects have been culled from both data sets, but, as described in the text, it is impossible that 10 or more of the faint ($R_F > 20.5$) blue [$(B_J - R_F) < 1.0$] objects are QSOs or CNELGs.

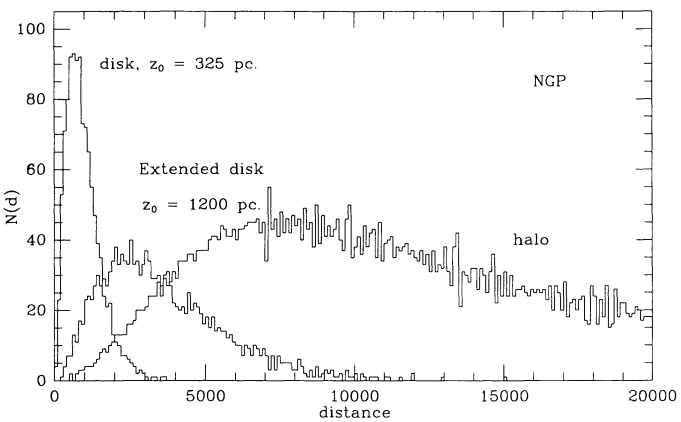

FIG. 3.—Distance distributions (from the "standard" model) of the three subpopulations identified in Figure 2*b*. The data plotted are for halo stars with $4.5 < M_v < 6.5$ and disk and E/T disk "stars" with $7 < M_v < 9$, but the shapes of the distributions are invariant with absolute magnitude (although the distance limit clearly depends on the absolute magnitude of the sample). Note the small range in distance described by the old disk as compared with the much broader halo distribution.

absolute magnitude ($M_v \sim +4$ to $+6$, near the main-sequence turnoff) and color (hence the blue peak in the model). At $V = 17$, the typical disk star is an early M dwarf, $M_v \sim +8$, while at $V = 22$ one is predominantly sampling near the peak of luminosity function, at $M_v \sim +12$. With a color index such as $(V-I)$, a sensitive absolute magnitude indicator to $M_v \sim +18$, the trend in M_v would be evident, since the mean color would become progressively redder at fainter magnitudes. $(B-V)$, however, saturates at a color of ~ 1.6 mag (equivalent to $M_v \sim +8$), leading to the conflation of stars at this color for magnitudes fainter than $V = 17$.

The blue edge in Figure 2*a* marks the turnoff color of the halo and is constant at $(B-V) = 0.4$ to $V \sim 21$. Fainter than this magnitude, the edge is less well defined. It is likely that this simply marks the increased photometric uncertainties of our observations, and a small color term is by no means ruled out at these very faint magnitudes. However, we emphasize that the conclusions drawn from our comparisons with the models are unaffected by such considerations, since these conclusions rest almost exclusively on analysis of the magnitude range $17 < V < 21$.

TABLE 3B

SA 57 STAR COUNTS AND *BV* DATA

	(B−V)										
V	0.1	0.3	0.5	0.7	0.9	1.1	1.3	1.5	1.7	1.9	2.1
16.10.....			1	1							
16.30.....			1		1						
16.50.....		1	1	2	2	1	1				
16.70.....			4	1				3			
16.90.....			4	1		1		2			
17.10.....			4	4	3	1	1				
17.30.....			6	1		1		2			
17.50.....		2	2	2	3	2	1	5			
17.70.....			4			1	3	5			
17.90.....	1	2	2	1	3	4	3	5			
18.10.....	2	3	2	2	2		2	3			
18.30.....		4	3	1	1	3					
18.50.....			1	1	4		2	3			
18.70.....			4	2	4		2	2	3		
18.90.....			2	2	1	2	5	4	1		
19.10.....			2	1	4	2	1	10	2		
19.30.....		1	2	2	2	1	3	7			
19.50.....			2	2	1			5	3		
19.70.....			5	3	4	2	2	4	3		
19.90.....		3	6	2	3		3	8	6		
20.10.....	1		7	2			2	8	4		
20.30.....			8	2	1		3	14	5		
20.50.....		1	6	2	1	3	5	7	3		
20.70.....			9	5	3	2	2	10	3		
20.90.....	1		7	6	6	7	4	16	5		
21.10.....		3	6	6	7	2	6	13	9		
21.30.....	1	1	9	5	5	3	4	20	6		
21.50.....			4	7	6	6	6	12	3		
21.70.....		1	3	8	6	3	5	17	9		1
21.90.....		1	7	13	7	4	6	10	12	1	
22.10.....	3	4	4	16	7	4	8	10	6		

NOTE.—The SA 57 star counts transformed from the *JF* passbands to *BV* using the transformations given by SRM.

Figure 4*a* compares the total *V*-band number counts predicted by this model with the observed distributions, where the counts at brighter magnitudes ($V < 18$) are from Reid's (1990) Oschin Schmidt north Galactic pole survey; these counts are in good agreement with Stobie & Ishida's (1987) Kiso Schmidt data (their Table III), which are tabulated only at 0.5 mag intervals. The fainter data are taken from SRM. Both sets of Schmidt data are limited to $V < 19$ (indeed, the Kiso Schmidt data become incomplete at $V = 18$), while the small solid angle covered by the SA 57 data leads to significant sampling uncertainties brighter than $V \sim 19$. As Majewski (1991) has pointed out, the region of overlap between the deep 4 m plate surveys and the Schmidt surveys, the magnitude range $\sim 18 < V < \sim 20$, has not received the observational attention it requires. Nonetheless, the agreement between the model and the data is well within the uncertainties of the observations, at least to $V \sim 20.5$ (we emphasize the point made in § 2.2. that there probably remains some residual contamination by stellar-like QSOs and CNELGs for $V \geq 21.5$). The wheels come off, however, when one compares the details of the observed and predicted color distributions (Fig. 4*b*–4*g*). (We use the Kiso Schmidt data in preference to the Oschin Schmidt data, since the former calibration is based on more plates.)

There are two striking discrepancies: the model *underpredicts* substantially the number of red (disk) stars at faint magnitudes and, to match the observed counts, compensates by *overpredicting* the halo star contribution. We have quantified the discrepancies between the model and the SA 57 data in Table 4B, where we list the number of stars per square degree for the three color ranges [$(B-V) = 0.3$–0.6, 0.8–1.1, and >1.4.] for 1 mag intervals between $V = 18$ and $V = 21$. (This magnitude range is *unaffected* by the possible color term we noted above.) The uncertainties listed are those corresponding to Poissonian statistical errors in the SRM SA 57 counts. In broad terms, the bluest bin includes mainly halo stars, the reddest bin is disk-dominated, while the intermediate colors probe predominantly the E/T disk. The standard model (model *a*) predicts 50%–100% too many blue stars and a factor of 2 too few red stars.

Considering the color distributions in detail, at brighter magnitudes ($V < 17.5$) the blue peak of the observed distribution lies ~ 0.15 mag to the red of the model predictions. In the model, the blue edge is set by the turnoff color of the halo population—that is, the turnoff color of M3. This discrepancy has been noted before—for example, in the Basel SA 57 data (Bahcall et al. 1985)—and, generally, has been resolved by adopting a halo color-magnitude diagram based on the metal-rich globular 47 Tuc. This results in an uncomfortable inconsistency, since the implied mean abundance is [Fe/H] ~ -0.7 for halo stars at distances of more than 5 kpc above the disk—in poor accord both with the local halo subdwarfs (which define the density zero point and have typical abundances of [Fe/H] ~ -1.3 to -2 [Laird et al. 1988]) and with the field star observations by Suntzeff et al. (1991) and by Kraft et al. (1992). Moreover, the E/T disk distribution plotted in

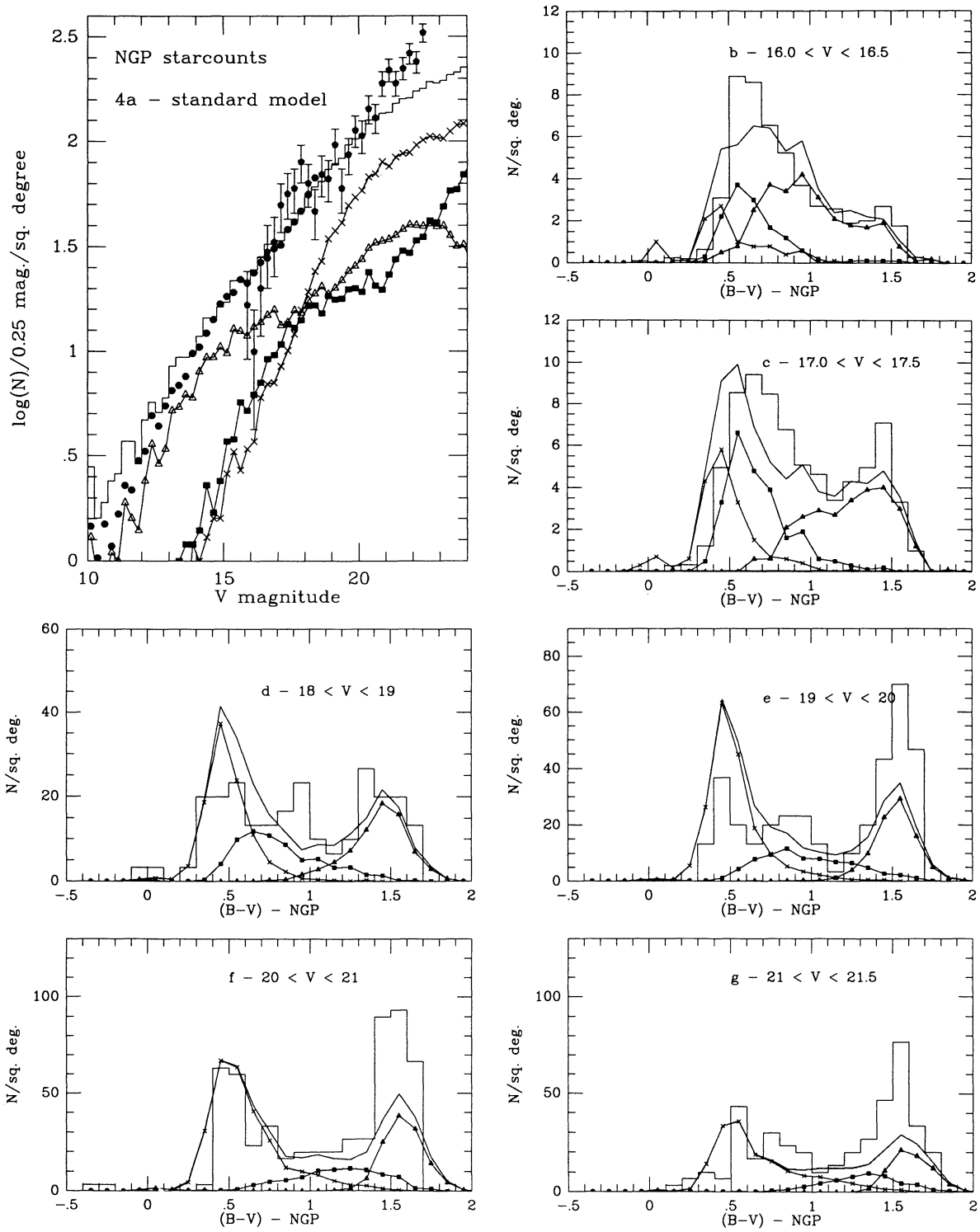

FIG. 4.—(*a*) Integral star counts toward the north Galactic pole predicted by the standard model. The contributions of the three components (halo, old disk, and E/T disk) are identified using the same symbols as in Fig. 2 (the young and intermediate disk make negligible contributions). The observed counts at brighter magnitudes (to $V = 18$) are from Reid (1990)—these data are in good agreement with the Kiso Schmidt observations by Stobie & Ishida (1987)—while the fainter counts are from the SRM SA 57 data set. We have plotted error bars to represent the Poissonian counting uncertainties in the latter observations; the corresponding uncertainties for the Schmidt data are smaller than the symbols plotted. (*b*, *c*) Color distributions predicted by the model matched against the Kiso Schmidt observations for two magnitude intervals. (*d–g*) Color distributions predicted by the model matched against the SRM SA 57 observations for four fainter magnitude intervals. Note the striking failure of the model, which predicts the total differential counts with tolerable accuracy, to fit the color distributions.

Figures 4*b* and 4*c* shows that even a 47 Tucanae–like color-magnitude diagram lies to the blue of the observed peak—a point to which we shall return in more detail in § 4.2.2.

At fainter magnitudes, the model predicts a strongly bimodal distribution which is not actually observed until $V > 20$. It is our contention, which we discuss in full in the following section, that this stems from two sources: first, the model predicts too many halo stars, leading to an enhanced blue peak; second, the presence of a more populous, redder E/T disk component fills in the central part of the color distribution between 18th and 20th magnitudes, further reducing the prominence of the blue peak.

TABLE 4A

MODEL PARAMETERS

	HALO			E/T DISK			OLD DISK		
MODEL (1)	ρ_0 (%) (2)	c/a (3)	LF (4)	ρ_0 (%) (5)	z_0 (6)	CMD (7)	$z_0(1)$ (8)	$z_0(2)$ (9)	COMMENTS (10)
a	0.15	0.85	Std	2	1200	47 Tuc	325	325	"Standard"
b	0.15	0.85	GC	2	1200	47 Tuc	325	325	
c	0.085	0.85	Std	2	1200	47 Tuc	325	325	
d	0.15	0.6	Std	2	1200	47 Tuc	325	325	
e[a]	0.025	0.9	GC	2	1200	47 Tuc	325	325	H87
	0.27	0.5	GC						
f	0.2	0.7	GC	2	1200	47 Tuc	325	325	
g	0.15	0.8	GC	4	1000	47 Tuc	249	249	KG89
h	0.15	0.8	GC	11	940[2]	OD	270[b]	270[b]	S87
i	0.15	0.8	GC	1.0	2500	47 Tuc	325	400	
j	0.15	0.8	GC	4.0	1800	Mid	325	400	
k	0.15	0.8	GC	2.5	1400	Mid	325	400	Interim
l	0.15	0.8	GC	2.0	1600	Mid	325	400	
m[a]	0.15	0.8	GC	2.5	1400	Mid	325	400	SLZ90
	0.09	0.4	GC						
n	0.12	0.85	GC	2.5	1400	Mid	325	400	

NOTE.—Principal parameters for the sequence of models used to generate the $(B-V)$ data listed in Table 4B. (1) Col. (1) identifies the model. Cols. (2)–(4) list data for the halo—the local number density normalization, ρ_0 (expressed as a percentage with respect to the disk), the axial ratio (c/a), and the luminosity function (LF) (either the standard model [Std] or the GC function plotted in Fig. 5*e*). Cols. (5)–(7) give the local normalization (again relative to the local disk density) for the E/T disk the scale height (in parsecs), and the color-magnitude diagram. The last is based on 47 Tuc, on the nearby stars of the old disk (OD), or on an intermediate color-magnitude diagram (Mid) described in more detail in § 4.2.2. Cols. (8) and (9) list the scale heights adopted for old disk stars with $M_v < +9$ [$z_0(1)$] or $M_v \geq +9$ [$z_0(2)$]. Col. (10) identifies the "standard" model and those models which test the particular hypotheses of Hartwick 1987 (H87), Kuijken & Gilmore 1989 (KG89), Sandage 1987 (S87), and Sommer-Larsen & Zhen 1990 (SLZ90).

[a] These models have two halo components.

[b] The Sandage 1987 model does not employ exponential density laws. The values listed are the distances above the disk where the density law declines to $\rho = e^{-1}\rho_0$.

TABLE 4B

PREDICTED STAR COUNTS

	V = 18–19			V = 19–20			V = 20–21			
MODEL	(a) 63 ± 14	(b) 50 ± 13	(c) 81 ± 16	(a) 70 ± 15	(b) 60 ± 14	(c) 180 ± 24	(a) 126 ± 20	(b) 57 ± 14	(c) 277 ± 30	COMMENTS
a	95	28	52	141	40	88	163	54	148	"Standard"
b	64	28	52	91	38	90	103	53	148	
c	58	27	52	84	34	90	91	42	147	
d	68	28	52	74	37	90	72	47	147	
e	59	29	52	63	44	91	64	60	149	H87
f	68	30	52	85	42	91	91	56	148	
g	63	29	36	87	44	61	101	56	100	KG89
h	81	35	41	116	36	80	119	61	126	S87
i	134	34	63	175	67	129	155	132	213	
j	151	90	68	148	155	146	117	196	263	
k	72	38	65	94	60	136	102	71	228	Interim
l	82	38	65	101	65	134	107	89	224	
m	80	40	65	101	63	135	114	77	228	SLZ90
n	67	38	65	87	58	135	96	67	227	

NOTE.—The number of stars per square degree is given for three color ranges, designated as (a) $(B-V) = 0.3$–0.6, (b) $(B-V) = 0.8$–1.1, and (c) $(B-V) > 1.4$, at each of the magnitude intervals $V = 18$–19, $V = 9$–20, and $V = 20$–21. Beneath the color ranges are given the observed surface densities for the SA 57 field, and the associated uncertainties are derived from the Poissonian statistics. As Fig. 4 shows, these three color intervals sample (predominantly) the halo, the E/T disk and the old disk, respectively. Details of the individual models are given in Table 4A and in the text.

The success that previous models have shown in matching the star counts at bright ($V \leq \sim 17$) magnitudes reflects the fact that the *total* star counts at these magnitudes are still primarily due to the old disk; hence the predictions of the BS84 model, for example, prove a relatively good match to data from the Basel survey ($R \leq 17.2$; Bahcall et al. 1985). Inconsistencies start to become apparent at $V > 18$, but these are masked to some extent by the corresponding increase in the photometric uncertainties close to the plate limits (typically 19th magnitude for Schmidt data). With the new, high-accuracy, deep SA 57 photometry, however, it becomes clear that the "standard" model is not an accurate representation of the structure of the Galaxy. In the following section we test how varying some of the more important input parameters affect the model predictions.

4. THE STANDARD MODEL REEXAMINED

The main aim of this paper is to demonstrate the poor fit between the published, generally accepted models of the Galaxy and the SA 57 data. We have deep photometry for only this one field, so it is not possible to undertake a detailed study of every parameter that goes into building a star-count model. However, without aiming at a definitive result, we can use the available data to identify potential problem areas and at least set constraints on some of the more influential parameters. It is in this spirit that we discuss the new models which we have constructed.

4.1. *The Halo Problem*

We have shown that the "standard" model predicts significantly more halo stars than are observed in SA 57. There are at least three possible means of reducing the contribution of this population in the "standard" model. We deal with each of these separately in the following sections, although we recognize that the individual parameters are often strongly correlated (or anticorrelated) in interpreting the results of star-count models.

4.1.1. *Change the Shape of the Luminosity Function*

For our standard model we have adopted a halo luminosity function which matches the WJK disk $\Phi(M_v)$ at magnitudes fainter than the turnoff. This means that the function is nearly flat from $M_v \sim +4.5$ to $M_v \sim +8$. Combining this with the broad distance distribution (Fig. 2) leads to the field star counts brighter than $V \sim 23$ being dominated by stars within 2 mag of the turnoff. However, the majority of the local proper-motion stars which define the zero point of the luminosity function are significantly fainter ($M_v > +7$). Thus these observations do not represent a strong constraint on the number densities near the turnoff. Clearly, depressing the halo luminosity function for $M_v < \sim +6$ will reduce the predicted number of halo stars.

The form of the halo-star luminosity function can also be estimated using either theoretical models or globular cluster (GC) luminosity functions. With the development of CCD technology, substantial effort has been devoted in recent years to the latter problem. However, since the emphasis has been on studying the lower mass stars on the main sequence, few of these studies are well suited to our purposes. Most investigations are based on one or two small ($\sim 3' \times 5'$) fields in the outer regions of the clusters, where the star density is low enough to allow deep, accurate photometry. This means that the data include relatively few (typically 15–20) stars at or above the turnoff of the main sequence—the most important region for star-count work—and therefore we must average data from several clusters. We have also chosen to normalize the various functions together at $M_v = 6.25$, rather than, as in previous studies, right at the turnoff ($M_v = +4.5$), where stellar evolutionary effects may still be important.

Figure 5 compares some of the more recent analyses of globular cluster data with the theoretical luminosity functions derived from the Yale and the VandenBerg & Bell (1985) stellar models and the nearby-star analyses by Dawson (1986) and Bahcall & Casertano (1986). We have also plotted the luminosity function derived by Sandage (1957) for M3, based on photographic data covering the entire cluster; the WJK disk luminosity function scaled by a factor of 0.15; and the halo $\Phi(M_v)$ that we adopted for the "standard" model. We have included both the last function and the Sandage M3 luminosity function for reference in each of the panels of Figure 5.

Stars brighter than $M_v \sim +3.5$ make little contribution to the deep star counts. Nonetheless, it is clear that, as noted previously by Kraft (1989), the Sandage (1957) M3 function lies above (higher densities) the results of most of the other studies, including the more recent analysis of the same cluster by Paez et al. (1987). We note that the latter is based on data from four CCD fields on the outskirts of the cluster, while the original M3 investigation used plates taken on the Palomar 200 inch telescope and covers the entire cluster. (Indeed, only the NGC 5053, 47 Tuc, and M92 luminosity functions are based on photometry of a substantial fraction of each cluster.) Kraft (1989) has shown that one can match the observed number of blue horizontal-branch stars and halo giants both in the GR83 south Galactic pole field and in Hartwick's (1983) survey field if one adopts both the M92/NGC 5053/47 Tuc luminosity function (rather than the Sandage M3 data) and a Hess diagram that matches that of M3 or M5. The lower red giant densities are also in good agreement with Preston et al.'s (1991) estimate of the local density of horizontal-branch stars, with the paucity of halo giants found in Friel's (1987) Serpens field and with theoretical predictions (we note that Bergbusch & VandenBerg 1992 have recently shown that their most recent models provide an excellent fit to both the M92 and 47 Tuc luminosity functions).

Comparing the various globular cluster functions, it is clear that, allowing for the uncertainties, there is good agreement over the absolute magnitude range $3.5 < M_v < +7$. The one notable exception is Palomar 5, a distant cluster on a nearly radial orbit (Cudworth, Schweizer, & Majewski 1993) which may have undergone such severe dynamical evolution that the luminosity function peaks at $M_v \sim = +6$. We find that the average luminosity function is not as flat as the WJK function for $4 < M_v < 6.5$; thus, normalizing at $M_v = +6.25$ reduces the implied density at the turnoff by nearly a factor of 2.

This result is at variance with the sharply truncated form of the halo luminosity function that we (and most others; see, e.g., Fig. 6 of Gilmore 1984) adopted for the halo in our "standard" model. In quantitative terms, the standard model has a number density ratio ($M_v = +3 : +4.5 : +6.5$) of (1:60:60), while the revised function (plotted in Fig. 5*e*), which we shall refer to as the GC function, has ratios of (2.5:24:60). The cluster 47 Tuc, the most metal-rich cluster plotted in Figure 5, has the most abrupt break near the turnoff of the luminosity function, but even in this cluster, inappropriate as it is as a halo template, the number ratios are (1.5:23:60). We have also plotted the subdwarf luminosity functions derived by Dawson (1986) in

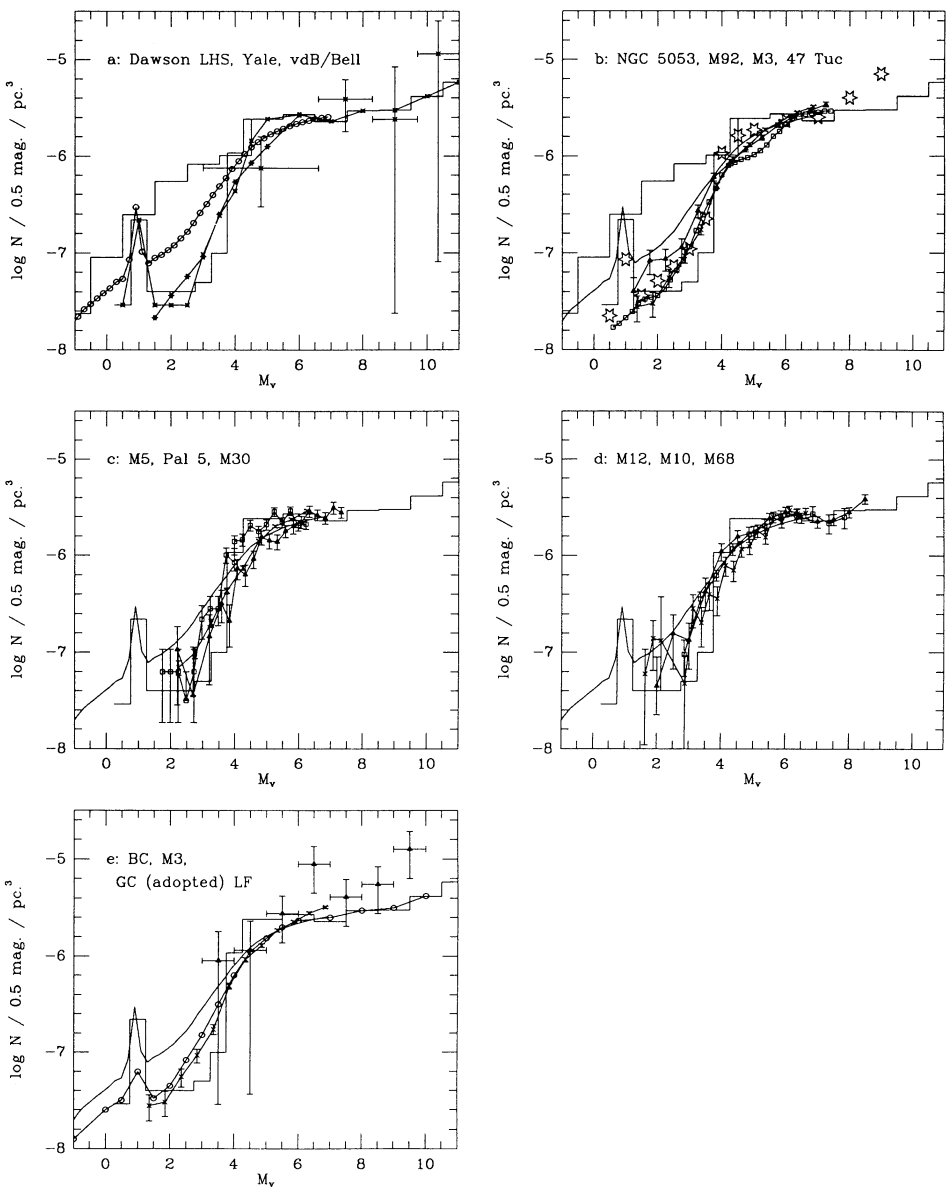

FIG. 5.—Estimates of the halo-star luminosity function. (*a*) Comparison of the disk luminosity function (scaled to 0.15% of the local density; *upper histogram*), the "standard" model [truncated WJK $\Phi(M_v)$] representation of the halo luminosity function (*lower histogram*), the Sandage (1957) M3 luminosity function (scaled to match the disk function at $6 < M_v < 7$; *open circles*), Dawson's (1986) luminosity function determination based on nearby LHS stars (*crosses with error bars*) and theoretical models. The latter are taken from the revised Yale tracks (Green, Demarque, & King 1987; *6-point stars*) and from the VandenBerg & Bell (1985) calculations (*4-point stars*). (*b*) Globular cluster luminosity functions for NGC 5053 (*filled triangles*) from Fahlman, Richer, & Nemec (1991); M92 (*open squares*) from Bergbusch's (1990) compilation of data from Tayler (1954), Hartwick (1970), van den Bergh (1975), Fukuoka & Simoda (1976), Sandage & Katem (1983), and Stetson & Harris (1988); M3 (*crosses*) from Paez, Straniero, & Martinez Roger (1990); and 47 Tuc (*6-point stars*) from Bergbusch & VandenBerg (1992), combining results from King, Da Costa, & Demarque (1985) and Hesser et al. (1987). Zinn & West (1984) cite abundances of −2.58 for NGC 5053, −2.24 for M92, −1.66 for M3 (but see text), and −0.71 for 47 Tuc. The scaled disk luminosity function, the standard model halo luminosity function, and Sandage's M3 function are also plotted for reference. The differences between the last and the Paez et al. results are discussed in the text. (*c*) Cluster luminosity functions for M12 (*triangles*) from Sato, Richer, & Fahlman (1989); M10 (*open squares*) from Hurley, Richer, & Fahlman (1989); and M68 (*crosses*) from McClure et al. (1987). The abundances from Zinn & West (1984) are −1.61 for M12; −1.60 for M10; and −2.09 for M68. Again, we plot the Sandage M3 function and the standard model halo function as references. (*d*) Cluster luminosity functions for M5 (*triangles*) from Richer et al. (1991); Palomar 5 (*open squares*) from Smith et al. (1986); and M30 (*crosses*) from Piotto et al. (1987). The abundances from Zinn & West (1984) are −2.40 for M5, −1.47 for Palomar 5, and −2.13 for M30. (*e*) Filled triangles show the subdwarf luminosity function derived by Bahcall & Casertano (1986), who applied Schmidt's V/V_{max} method to a sample of proper-motion stars. The mean local halo-to-disk ratio that they derive is ∼0.35% (§ 4.1.2), but in this context we are concerned only with the shape of the distribution. We also plot the luminosity function that we have adopted for the halo as the average of the various globular cluster studies—the GC function (*circles*). Again, we plot the Sandage and Paez et al. M3 luminosity functions and the standard model halo luminosity function for reference.

Figure 5*a*, and those described by Bahcall & Casertano (1986) in Figure 5*e*; note that the brightest bin of the Luyten Half-Second Catalogue (LHS) data set (Luyten 1976) includes the magnitude range $3.0 < M_v < 6.6$, and that the latter function is normalized to 0.35% of the local disk density. Both, however, are more consistent in shape with the GC luminosity function rather than the flat WJK disk function for $M_v < +7$.

Incorporating the GC luminosity function in the "standard" model leads to a significant reduction in the predicted number of halo stars in SA 57. Table 4 (model *b*) shows the effect on the total number of blue stars predicted; the counts fall to within 2 σ of the observations [for ρ_0(halo) = 0.15% ρ(disk), $c/a = 0.85$]. The full $(B-V)$ distributions at $V = 18$ and $V = 20$ are plotted in Figures 6*a* and 6*b*.

4.1.2. *Change the Normalization of the Luminosity Function*

The number of halo stars predicted at a given apparent magnitude obviously scales directly with the local number density (often expressed as the number ratio relative to disk stars) that is adopted. Figures 6*c* and 6*d* (and Table 4, model *c*) show that reducing the local halo normalization in the "standard" model by a factor of 2 (a halo/disk ratio of 0.085%) gives better agreement with the observations. As we described in § 3.3.1, this quantity is derived primarily from samples of proper-motion stars, although other indicators such as horizontal-branch stars and RR Lyrae stars are consistent with a normalization in the range 0.15%–20%. The proper-motion sample analyses, whether based on selecting stars with tangential velocities greater than a certain limit (Schmidt 1975); Rich-

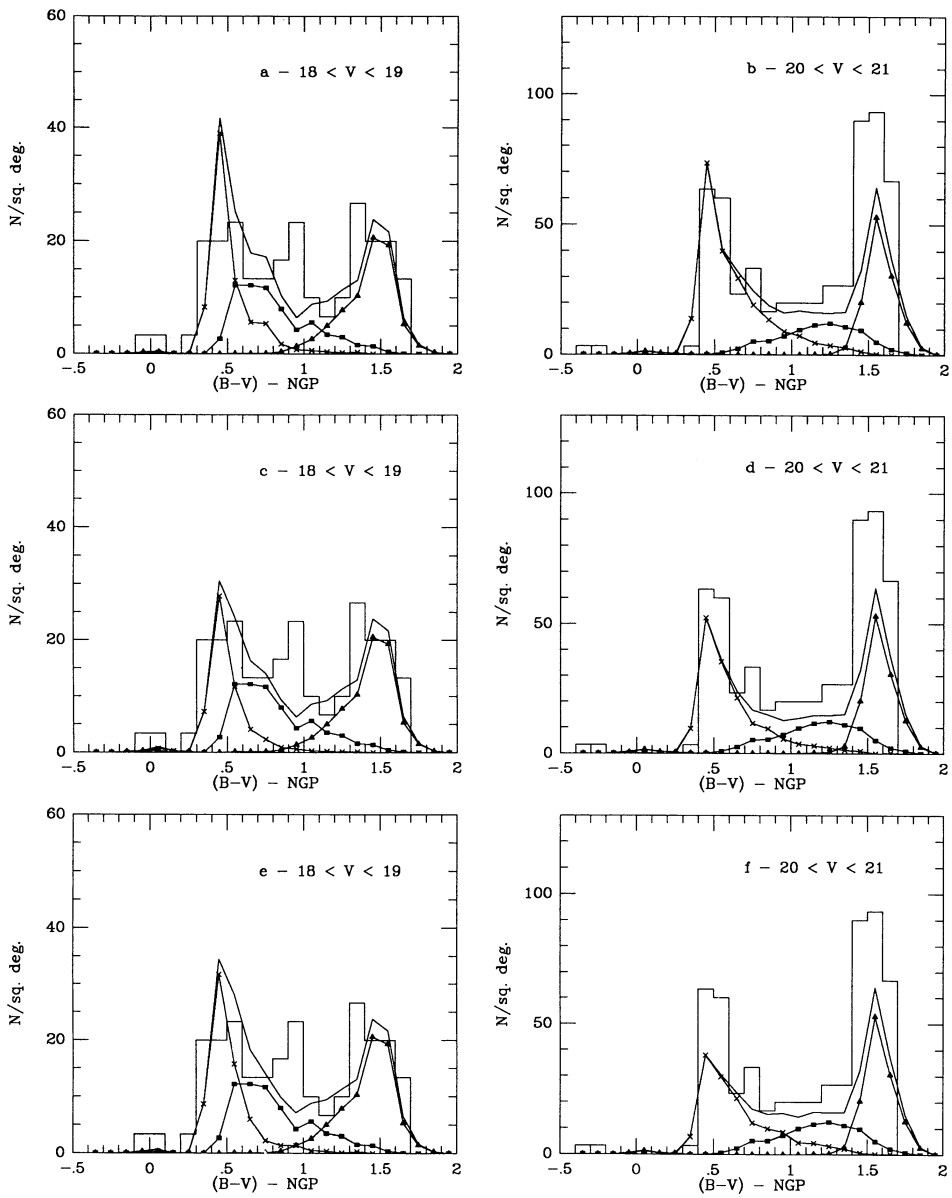

FIG. 6.—Reconciliation of the observed and predicted halo distributions through different mechanisms. (*a*, *b*) Predicted color distributions at $V = 18$–19 and $V = 20$–21 if one adopts the GC luminosity function for the halo; the histogram plots the SRM SA 57 observations (model *b*, Table 4). (*c*, *d*) Standard model luminosity function with a local normalization of 0.085% of the number density of the disk stars (model *c*, Table 4). (*e*, *f*) Standard model luminosity function, a local halo-to-disk ratio of 0.15%, and an axial ratio c/a of 0.6 (model *d*, Table 4).

stone & Graham 1981; Bahcall & Casertano 1986) or on use of the reduced proper-motion diagram (Dawson 1986), require that one adopt a particular set of kinematics for the halo. Given the kinematics, one can apply Monte Carlo techniques to estimate the fraction of halo subdwarfs included in the sample (and the extent of contamination by disk stars) and then correct the observations to derive a local number density.

However, the effective distance limit for a proper-motion limited sample varies linearly with the mean transverse velocity, V_t, so the inferred local number density varies as $\langle V_t \rangle^3$ (Reid 1984). Thus the density estimates are strongly dependent on the kinematic model adopted for the halo; indeed, this accounts for the fact that Bahcall & Casertano (1986) derive a local halo number density of 9.5×10^{-5} stars pc^{-3} ($4 < M_v < 11$), or 0.37% ρ_0(disk), while Dawson (1986) derives a normalization of only 0.17% ρ_0(disk).

We have used Monte Carlo simulations to test how changing the assumed halo kinematics affects the deduced halo/disk ratio. Table 5 shows Dawson's LHS discovery fraction for a representative range of kinematics. These results show that the mean system rotation adopted is a very important parameter; analyzing the LHS data based on the kinematics that Bahcall & Casertano (1986) adopt for the halo reduces the discovery fraction [and hence increases the inferred ρ_0(halo)] by nearly a factor of 2 (Table 5, line B). Analyses of RR Lyrae stars (lines A and C), subdwarfs (lines D and E), and metal-poor giants (line F) imply a net prograde rotation of 20–40 km s^{-1} for the halo and local densities of ρ_0(halo) = 0.17%–0.24% ρ_0(disk). On the other hand, using the halo kinematics derived in the two deep proper-motion studies (retrograde halo rotation; lines G and H in Table 5) leads to ρ_0(halo) = 0.11%–0.13% ρ_0(disk).

However, to reduce the local halo/disk ratio to 0.085%—the normalization required if we retain the "standard model" halo luminosity function—demands extremely hot halo kinematics (Table 5, lines I and J). If we adopt normal velocity dispersions (i.e., use the metal-poor RR Lyrae stars as tracers), then we require a solar motion of $V \sim -325$ km s^{-1} (100 km s^{-1} retrograde motion), while even the mildly retrograde halo deduced from the analysis in SRM requires markedly higher dispersions than are observed for any standard halo tracer. Thus one cannot reconcile the "standard model" with the observations by simply renormalizing the local halo density without creating other significant inconsistencies.

TABLE 5

HALO KINEMATICS AND THE LHS CATALOG

Source (1)	U (2)	V (3)	W (4)	σ_U (5)	σ_V (6)	σ_W (7)	f_{LHS} (%) (8)	h/d (%) (9)
A	0	−220	0	145	125	71	6.6	0.17
B.....	0	−154	0	140	100	76	3.5	0.32
C	−24	−180	−6	157	104	91	5.1	0.21
D	0	−190	0	131	106	86	4.8	0.23
E.....	32	−206	−8	154	102	107	5.9	0.19
F.....	0	−195	0	133	98	94	4.6	0.24
G	0	−275	0	145	125	71	10.0	0.11
H	0	−250	0	145	125	71	8.1	0.13
I	0	−325	0	145	125	71	12.9	0.085
J	0	−275	0	185	155	110	13.2	0.085

NOTE.—The "LHS discovery fraction" (as defined by Dawson 1986) of local halo stars as a function of the kinematics assumed for the halo. Cols. (2)–(4) list the adopted solar motion; cols. (5)–(7) gives the velocity dispersion; col. (8) lists the percentage of stars within 300 pc of the Sun which have tangential motions sufficient to ensure inclusion in the Luyten Half-Second Catalogue ($\mu > 0''$, 5 yr^{-1}); col. (9) gives the inferred local halo-to-disk ratio (again expressed as a percentage). The kinematics listed are taken from several sources: Line A from Woolley's 1978 statistical parallax analysis of metal-poor RR Lyrae stars; line B from Bahcall & Casertano's 1986 analysis; line C from Strugnell et al.'s (1986) statistical parallax analysis of metal-poor RR Lyrae stars; line D from the analysis of the local subdwarf kinematics by Norris 1986, and line E from Carney & Latham's 1986 and line F from Morrison et al.'s 1990 study of metal-poor giants; the halo solar motion in line G is from the SA 57 proper-motion study by SRM; the halo solar motion in line H is from Reid's 1991 analysis of proper motions in the north Galactic cap. Finally, lines I and J illustrate the type of kinematics which is required if the standard model is to match star-count observations.

4.1.3. *Change the Halo Density Law*

The number of halo stars at $2 \geq 5$ kpc can be reduced either by changing the slope of the density distribution or by adopting a flatter c/a axial ratio for the same density law. Given that we have data for only one field, and bearing in mind that all the available observations (as discussed in § 3.3.1) indicate a density law no steeper than $r^{-3.5}$, we have restricted ourselves to varying the axial ratio. However, even within this one field we have some leverage on the halo distribution, since the star counts require that the number of halo stars increase between 18th and 21st magnitude. Hence, while we can reconcile the standard model with the observations between $V = 18$ and $V = 20$ by adopting an axial ratio of $c/a = 0.6$, the model then underestimates the number of blue stars between $V = 20$ and $V = 21$ (Figs. 6*e* and 6*f*; Table 4, model *d*); that is, the gradient in the number counts requires that a significant fraction of the halo reside in a component with an axial ratio of ~ 0.8.[7]

Models with halos having an axial ratio of 0.8, the GC luminosity function, and a local density of 0.15% ρ_0(disk) (Table 4B, models *g*–*l*) match the observations to within 1 σ. As might be expected, one can trade off between local normalization and axial ratio—thus, an axial ratio of 0.85 matches the data for a local halo/disk model *l*). Taken at face value, these normalizations are in relatively poor agreement with the results listed in Table 5 that are derived from analysis of *local* samples of the halo stars (lines A, C, D, and E). However, if a significant fraction of the local halo stars have orbits that outline a flattened distribution ($c/a \sim 0.5$ or less), then these stars make little contribution to the densities at $z > 6$ kpc. In other words, the local density normalization that we infer from the star-count data reflects only the contribution of the more spherical component(s) in a multicomponent model. To give a specific example, if we accept the arguments in SLZ that ~40% of the local halo stars are in a more flattened distribution, then our results imply that the *total* local density of halo stars is between 0.20% and 0.25% ρ_0(disk). Model *k* in Table 4 models this double-component halo, and it is clear that the additional component has little impact on the counts. However, models based on Hartwick's two-component halo, which has a local space density ~0.3% ρ_0(disk) but places only 10% of the subdwarfs in a near-spherical distribution, fail to match the observations (Table 4 model *e*).

Finally, we noted in § 3.3.1 that Wyse & Gilmore (1989) derive an axial ratio of 0.6 for the halo as a whole from a comparison of the number of stars with $18 < V < 20$ and $(B-V) < 0.6$ in two 0.75 deg^2 fields toward the north Galactic pole and in UK Schmidt Telescope field 117 ($l = 272°$, $b = -44°$). Gilmore et al. (1989) discount axial ratios derived

[7] Elsewhere (Reid 1993) we derived a best-fit axial ratio of ~0.7, but this was for an adopted halo luminosity function that lay between the standard model and the Sandage M3 data, with $N(M_v = +3{:}+4.5{:}+6.5)$ of (5:32:60).

from the Kron SA 68 and SA 57 data. Since both E/T disk and halo contribute to the total counts at these magnitudes, the fraction of E/T stars must be inferred from models before deriving c/a. Our reanalysis of the south Galactic pole and SA 57 data in the following section suggests that larger scale heights/local normalizations should be used for the disk models than those adopted by Wyse & Gilmore. In that case, the disk (particularly the E/T disk) makes a larger contribution to the blue stars, decreasing the observed ratio between the pole and lower latitudes. Using our interim model (§ 4.3), we estimate allowing for disk-star contamination that their observed ratio of 0.59 is consistent with an *average* halo axial ratio of 0.75–0.8.

4.1.4. *Summary*

The main conclusion that can be drawn from the limited exploration of parameter space that we have undertaken is that the form that one adopts for the halo luminosity function near the turnoff is of crucial importance in interpreting the star-count data. (The halo luminosity function at faint magnitudes, $M_v \geq +8$, is essentialy irrelevant, at least for current star-count investigations.) None of the models listed in Table 4 provide a perfect match to the observations—nearly equal number densities of blue stars at $V = 18.5$ and $V = 19.5$, and a factor of 2 increase at $V = 20.5$. However, if we adopt the GC luminosity function for the field stars of the halo, we can match the SA 57 data to within 1 σ with a population having an axial ratio of 0.8 ± 0.05 and a local normalization of $\rho_0 = 0.15 \pm 0.03\%$ ρ_0(disk) (the normalization and axial ratio are anticorrelated). The *total* local density of halo subdwarfs may be higher if multicomponent models of the halo, such as that proposed by Sommer-Larsen & Zhen (1990), are correct.

4.2. *The Disk Problem*

In contrast to the case of the halo, the disk star contribution to number counts at faint magnitudes is underestimated by the "standard" model. The same defect afflicts the predictions of models which base the parameters of the disk populations on the studies by Sandage (1987) and by Kuijken & Gilmore (1989). As we described in § 3.2.1, the latter analyze the density distribution of K dwarf stars toward the south Galactic pole, finding scale heights of 249 pc for the old disk and 1000 pc for the E/T disk, with the relative normalization locally being 96:4. (The normalization of the E/T disk is anticorrelated with scale height; that is, adopting a larger scale height for the old disk leads to a larger inferred scale height for the E/T disk, but a lower normalization.) Figure 7 and Table 4 (model g) show that a model with these parameters fails to match the number of faint ($V > 19$) red stars by nearly a factor of 3.

Sandage's (1987) characterization of the vertical density distribution, as we described in § 3.2.2, is derived from his application of Kapteyn's (1922) equation relating the density distribution, $D(z)$, to the velocity dispersion, σ_w, of a given component through the gravitational acceleration perpendicular to the plane, $g(z)$. Sandage uses Saio & Yoshii's (1979) derivation of the latter parameter. This method of calculation leads to density laws which fall off relatively slowly at low z and tend toward exponentials at high z. Hence, while the density of old disk stars ($\sigma_z = 17$ km s^{-1}) drops by $1/e$ within the first 270 pc, the scale height of the high-z exponential distribution is only $\sim$150 pc; the corresponding parameters are 940 and $\sim$635 pc for the E/T disk ($\sigma_z = 42$ km s^{-1}) and 3200 and $\sim$2850 pc for the halo ($\sigma_z = 90$ km s^{-1}). The relative normalizations (200:22:1–disk:E/T disk:halo) are then set by matching the density distribution of $M_v = +4$ stars [0.3–0.6 in $(B-V)$] toward the Galactic pole (from observations by GR83, Fenkart 1966, Yoshii et al. 1987, and Becker & Fenkart 1976). Following Sandage's analysis, we have used the nearby-star color-magnitude diagram, rather than 47 Tuc, for the E/T disk in this model. The results are plotted in Figure 8 (Table 4, model h). Although the peak in the color distribution is a reasonable match to the observations at intermediate magnitudes ($V \sim 15$–17), the steep density laws lead to too few M dwarfs at faint magnitudes.

Thus, none of the extant models are capable of fitting the deep SA 57 color distributions. In the following sections we reconsider the derivation of the disk density laws.

4.2.1. *The Disk Density Laws*

The scale height of 325 pc used for the old disk in the standard model is based on the results presented in Figure 5 of GR83. The density laws were derived by applying the method of photometric parallaxes—specifically the $[M_v, (V-I)]$ relation—to the south Galactic pole data. Stobie, Ishida and Peacock (1989, hereafter SIP89), however, have shown that the spline fit used in GR83 is a poor match to the most recent observations of nearby stars with known trigonometric parallax. In fact, the color-magnitude diagram for K and M dwarfs can be described by a linear relation,

$$M_v = 2.89 + 3.37(V-I)\,, \quad (V-I) > 0.92$$

(SIP89; Reid 1991), while at brighter absolute magnitudes the relation

$$M_v = 1.10 + 5.33(V-I)\,, \quad 0.5 < (V-I) < 0.02\,,$$

gives a close approximation to the color-magnitude relation. (These relations are valid for near-solar abundance. We discuss the effects of metallicity variations in the following section.) We have therefore rederived the vertical density laws from the south Galactic pole data using the corrected relation (Fig. 9). However, before discussing our results we consider the matter of contamination of the sample by distant halo giants.

Any photometric parallax analysis rests on the assumption that the overwhelming majority of stars in the sample conform to the (absolute magnitude, color) relation that is being applied; in our case we assume that the sample is dominated by dwarf stars. This assumption has been questioned (Bahcall 1986), but we can use our model to demonstrate that our assumption is valid. Figure 10 shows the predicted color-magnitude diagram for halo stars with $M_v \leq +3.5$; the data are taken from model k in Table 4 (although note that models g–l all have the same halo parameters) and are for a solid angle of 10 deg^2. We have marked the $(V-I)$ limits appropriate to the $5.5 \leq M_v < 6.5$ sample, and the predicted contamination is clearly minimal: fewer than 5 stars deg^{-2} for $13 < V < 18$ as compared with observed surface densities of 5.6 stars deg^{-2} at $V = 13.5 \pm 0.5$ and 33.0 stars deg^{-2} at $V = 17.5 \pm 0.5$. This is not surprising, since these color limits span the base of the giant branch in M3 and therefore include stars with absolute magnitudes in the range $\sim +2.5$ to ~ 0. Observational support for a low surface density of halo giants comes from the Ratnatunga & Freeman (1989) survey and from Kuijken & Gilmore's (1989) K star observations. The former survey, although effectively limited to $(B-V) > 0.9$ or $M_v \geq 0$, found only 150 giants in 60 deg^2 while the latter, although deriving a higher giant/dwarf ratio ($\sim$25%) for $V < 16$, $(B-V) < 1$ (i.e.,

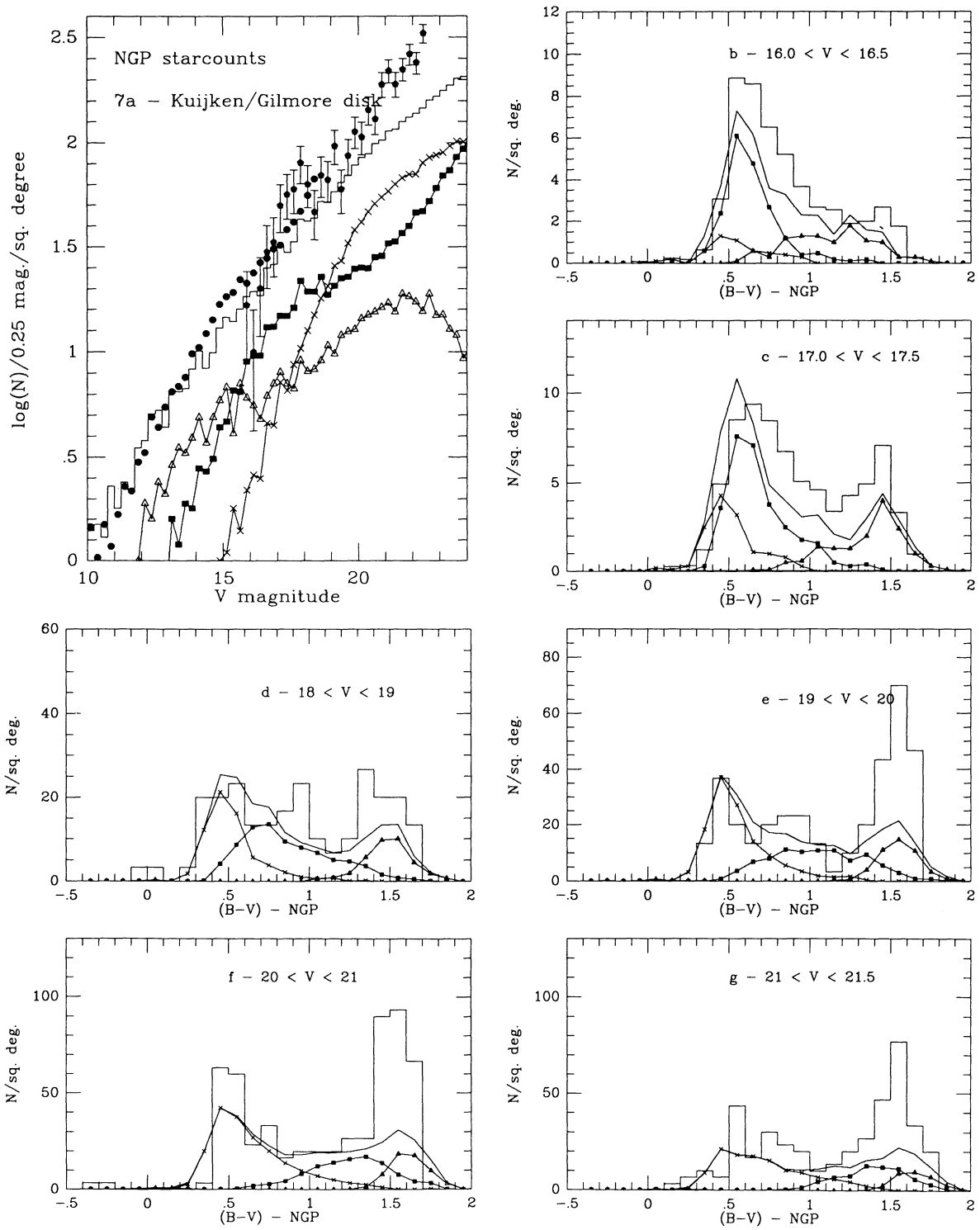

FIG. 7.—Predicted star counts and color distributions for a model including the standard halo, but with the old disk and E/T scale heights determined by Kuijken & Gilmore (1989) from their analysis of K dwarf stars. The symbols have the same meanings as in Fig. 4. The model underestimates severely the number of disk stars at faint magnitudes.

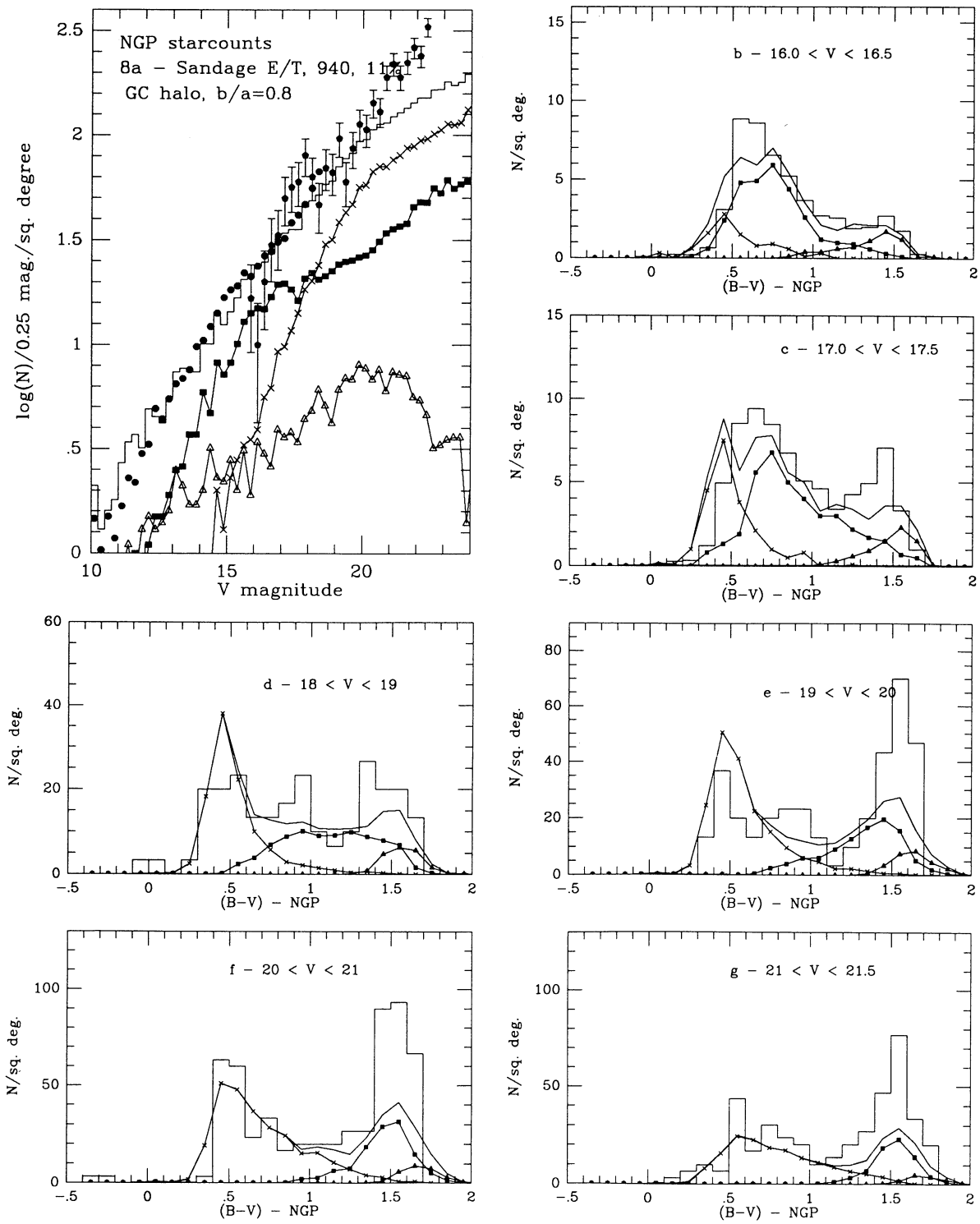

FIG. 8.—Predicted star counts and color distributions for a model matching the density distributions determined by Sandage (1987) from adopted velocity dispersions perpendicular to the plane for a disk, thick disk, and halo. Following the example of Sandage (1987), we use the nearby-star (old disk) color-magnitude relation for the E/T disk. Again the steep density laws lead to the model being unable to match the observed distribution at faint magnitudes.

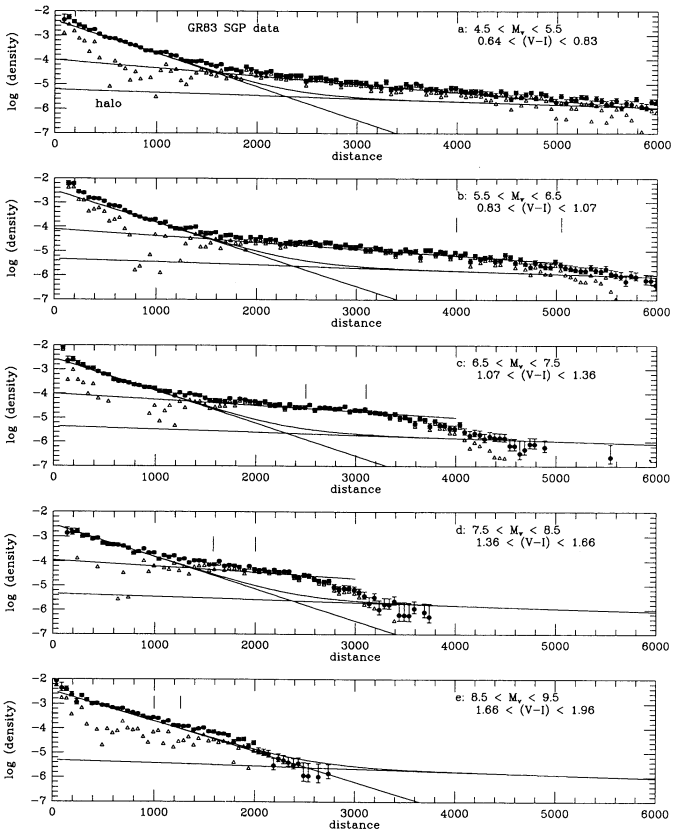

FIG. 9.—Density distribution derived by applying the photometric parallax method of analysis to the GR83 *VI* south Galactic pole photometry. The solid points show the observations, with the error bars corresponding to the Poissonian uncertainties. The two vertical lines plotted on each panel identify the distance at which the lowest luminosity stars in each sample have apparent magnitudes of $V = 19.5$ and $V = 20.0$. We have subtracted from the observations the contributions from both the $\sim$325 pc scale height old disk and the halo, modeling the latter as a 3500 pc scale height exponential normalized to 0.15% of the local disk density, and the residuals are plotted as triangles. There is a clear excess over the model at heights between $\sim$1.2 and $\sim$5 kpc. We have fitted (by eye) exponentials to these residuals, as a qualitative, rather than quantitative, indicator of the extent of the excess, and the resulting scale heights and local normalizations are listed (with the old disk parameters) in Table 6A.

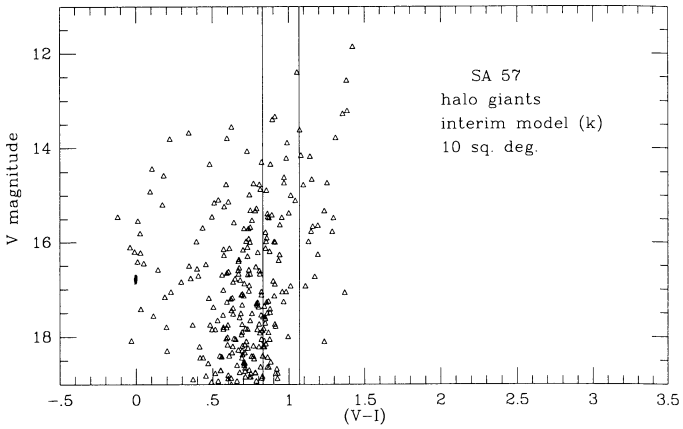

FIG. 10.—Color-magnitude diagram predicted for halo giants ($M_v < 3.5$) based on our interim model (model *k* in Table 4). This adopts the GC luminosity function, an axial ratio of 0.8, and a local normalization of 0.15% ρ(disk). The color limits plotted are for visual absolute magnitudes of +5.5 and +6.5.

$r < 1$ kpc; Fig. 9*b*), finds contamination to be no more than a few percent among redder and fainter stars.

To reinforce this point, suppose that the number density of $0.83 \leq (V-I) < 1.07$ stars *apparently* at 3 kpc in Figure 9*b* is actually due to distant halo giants. In that case we can calculate the required space density explicitly. Since the giants are $\sim$4 mag brighter than the main sequence at these colors, the distances are underestimated by a factor of 6 and the density by 6^3, so we derive an implied density of $\sim 10^{-7}$ stars pc^{-3} at $r \sim 18$ kpc. With an $r^{-3.5}$ density law, the *local* density is then $\sim 3 \times 10^{-6}$ stars pc^{-3}. This compares with the local density $\rho_0 \sim 2 \times 10^{-7}$ stars pc^{-3} for $M_v < +2.5$ that we derive from the GC luminosity function plotted in Figure 5*e*—that is, we can match the observations only by increasing the local density of halo stars by a factor of 10.

Halo star contamination is more noticeable at bluer colors [the $4.5 \leq M_v < +5.5$, $0.64 \leq (V-I) < 0.83$ sample], but even there the contribution is only $\sim$3 stars deg^{-2} between 16th and 17th magnitudes where the observed surface density is 27.6 stars deg^{-2}. Note that this magnitude interval corresponds to distances of at least 2500 pc, that is, *beyond* the change in slope of the density laws in Figure 9 (hence halo stars are not responsible for this feature in the density laws). The increased, although still insignificant, contribution of halo stars at these bluer colors follows from the longer lifetimes of stars on the subgiant (as opposed to the giant) branch. Contamination by evolved stars is negligible, however, for colors redder than $(V-I) \sim 1.1$, unless one chooses to invoke a halo with a substantial population of 47 Tuc (or more metal-rich) stars, or a strikingly rich asymptotic giant branch.

Figure 9 plots the density laws that we derive for stars in the absolute magnitude range $4.5 < M_v < 9.5$.[8] The vertical bars in each plot mark the distance at which the intrinsically faintest (reddest) objects in each sample have apparent magnitudes of 19.5 and 20.0. It is likely that our sampling becomes incomplete between these two points, particularly for the bluer stars, where the *I*-band limit of $I \sim 18.25$ comes into play. It should also be borne in mind that while the density distributions derived for the more luminous ($M_v < 6.5$) stars extend to larger distances, the steepening of the color-magnitude relation means that the individual distances are correspondingly more uncertain.

Considering first the inner portion of the density distributions, we find that the data can be represented to moderate accuracy with exponentials. The scale heights and extrapolated density at $z = 0$ are listed in Table 6; the latter values are broadly consistent with the WJK luminosity function. The apparent upturn in number density close to the Galactic plane ($z < 400$ pc) reflects contamination by disk giant stars at bright ($V < 13$) magnitudes. The average scale height is close to the 325 pc that we adopt in the standard model, although the faintest stars may better fit a slightly higher value.

At larger distances (>1 kpc) above the plane we find the same change in gradient in the stellar densities that was highlighted in GR83. The contributions of both the old disk (represented by the relevant exponential) and the halo have

[8] We have not allowed for binarism in the sample, but Kroupa, Tout, & Gilmore (1992) show that this has the effect of *underestimating* (by $\sim$15%) the true density gradient.

TABLE 6

THE SOUTH GALACTIC CAP DENSITY DISTRIBUTIONS

Magnitude Range (1)	Old Disk ρ_0 (stars pc^{-3}) (2)	z_0 (3)	E/T Disk ρ_0(E/T) Relative to Old Disk (%) (4)	z_0 (5)
A. No Abundance Gradient				
$4.5 \le M_v < 5.5$.....	4.1×10^{-3}	320	2.2	1300
$5.5 \le M_v < 6.5$.....	3.1×10^{-3}	330	2.6	1580
$6.5 \le M_v < 7.5$.....	3.0×10^{-3}	325	3.4	1740
$7.5 \le M_v < 8.5$.....	3.1×10^{-3}	330	3.2	1700
$8.5 \le M_v < 9.5$.....	3.4×10^{-3}	350	...	...
B. -0.10 dex kpc^{-1} Abundance Gradient				
$4.5 \le M_v < 5.5$.....	4.2×10^{-3}	320	2.7	1350
$5.5 \le M_v < 6.5$.....	4.6×10^{-3}	310	2.4	1400
$6.5 \le M_v < 7.5$.....	3.1×10^{-3}	315	3.7	1830
$7.5 \le M_v < 8.5$.....	3.2×10^{-3}	325	4.1	1750
C. -0.25 dex kpc^{-1} Abundance Gradient				
$4.5 \le M_v < 5.5$.....	4.2×10^{-3}	350	1.8	1930
$5.5 \le M_v < 6.5$.....	4.7×10^{-3}	310	1.4	2670
$6.5 \le M_v < 7.5$.....	2.9×10^{-3}	330	3.5	2480
$7.5 \le M_v < 8.5$.....	3.0×10^{-3}	350	3.8	2600

NOTE.—The exponential density distributions matched against the south Galactic pole field star counts plotted in Figs. 10 (no abundance gradient) and 12 (gradients of -0.10 and -0.25 dex kpc^{-1}). The scale height and extrapolated local density are listed for the old disk in cols. (2) and (3); col. (4) lists the density normalization of the exponential matched against E/T disk [expressed as a percentage of ρ_0(disk)]; and the E/T disk scale height is given in col. (5).

been subtracted from the total counts, and the residuals are plotted in Figure 9. These "excess" stars broaden the blue peak in the $(B-V)$ distribution for $V > 18$, weaken the predicted bimodality by filling in the intermediate colors, and contribute to the red peak at faint magnitudes. Note that they are the *dominant* contributor of "blue" $[(B-V) < 1]$ stars at intermediate ($V = 15$–17.5) magnitudes. The density of the extended/thick disk stars does not become comparable to that predicted for the halo until reaching heights of 5–6 kpc above the plane—the same height at which SRM found a significant change in the distribution of both kinematics and ultraviolet excess, prompting his suggestion that the halo only dominates beyond this distance.

Based on the results presented in Figure 9, we deduce that the E/T disk has a larger scale height and (possibly) a higher density normalization than we adopted for our "standard" model. Table 6 lists the parameters we derive if we match exponentials to the stellar excess in Figures 9*a*–9*d* (the lowest luminosity sample becomes incomplete at distances of only just over 1 kpc). The normalizations are between 2.0% and 3.5% of the local disk density, with scale heights between 1300 and 1700 pc. Clearly, neither parameter is well-defined, and it is possible that the higher scale heights derived for the fainter stars arise from the lower distance limit rather than from any real differences. The current scale heights, however, are closer to the 1350–1450 pc originally suggested by GR83 than the less than 1 kpc values determined more recently. (We remind the reader that we are using the same data set as GR83, albeit with an improved photometric parallax calibration.) As we shall discuss in the following sections, both the number counts toward the north Galactic pole—specifically at intermediate (14th–17th) magnitudes—and the SA 57 color distributions are fitted better if we adopt density normalizations in the 2.0%–2.5% range. Nonetheless, computing the surface densities of the old disk and E/T disk we find that at least 10% of the total mass of the disk resides in the extended component.[9]

4.2.2. *The Color-Magnitude Relation for the E/T Disk*

The density laws calculated in the previous section were based on single $[M_v, (V-I)]$ relation—that is, there is an implied assumption of no significant abundance gradient perpendicular to the plane. Both the extended disk and the thick-disk models predict that a gradient in the *measured* mean abundance should be present; in the former case, the higher velocity dispersion (σ_w) components are drawn from the oldest stars in the disk and hence can be expected to have abundances of [Fe/H] ~ -0.5 or less (Norris 1987a), while the thick disk is characterized as having a mean abundance of [Fe/H] $= -0.6$ (Gilmore et al. 1989; Carney et al. 1989). However, there is probably a significant range in abundance, given the recent identification of metal-poor ([Fe/H] < -1) giants rotating with the disk (Morrison et al. 1990). In any event, the different fractional contributions of the two discrete components, old disk and thick disk, at different heights leads to a gradient in the mean abundance with z.

Most direct studies of the abundance gradient are limited to stars within 2 kpc of the plane; thus, the stars for which Gilmore & Wyse (1985) obtained CCD *UBV* data are almost all within 1 kpc, while the ultraviolet excess observations by Yoshii et al. (1987), from which they derive a gradient of -0.5 ± 0.1 dex kpc^{-1} extend only to 2 kpc distance. The most extensive studies are K giant surveys summarized by Yoss, Neese, & Hartkopf (1987) and the ultraviolet excess SA 57 observations by SRM. The former study derives a gradient of -0.4 dex kpc^{-1} to $z = 700$ pc, with a subsequent gradient of -0.18 dex kpc^{-1} to 8 kpc. Even this survey includes relatively few stars with $z > 2.2$ kpc, and there is a substantial dispersion about the mean, with solar abundance stars persisting to heights of more than 3 kpc above the plane, although Norris & Green (1989) have argued for lower metallicities for the last-mentioned stars. The SA 57 data, however, also provide evidence for a substantial dispersion in abundance (SRM, Figs. 29 and 30) and argue for a less steep gradient in [Fe/H] within the first ~ 6 kpc. The mean abundance between 2.5 and 5 kpc is [Fe/H] ~ 0.4 ($\delta_{0.6} \sim 0.1$), although stars as metal-poor as [Fe/H] $= -2$ are present. Above 5 kiloparsecs, which is close to the point where the E/T disk and halo meet in Figure 9, there is a sharp reduction in the number of metal-rich stars. Carney et al. (1989) also find evidence for a weak abundance gradient in their analysis of a sample of high proper motion stars.

What effect does adding a metallicity gradient have on our density-law calculations? We have recalculated the south Galactic pole density distributions including abundance gradients of -0.25 dex kpc^{-1} (matching the Yoss et al. 1987 data points) and -0.10 dex kpc^{-1} (more consistent with the SA 57 data). In both cases we set a lower limit of [Fe/H] $= -1$. Metal-poor stars are subluminous compared with the nearby-

[9] Kuijken & Gilmore (1989) derive an even higher mass ratio between the E/T disk and the old disk, but we have already shown that the scale heights of 250 and 1000 pc that they derive for the two components are in poor accord with the deep star-count data.

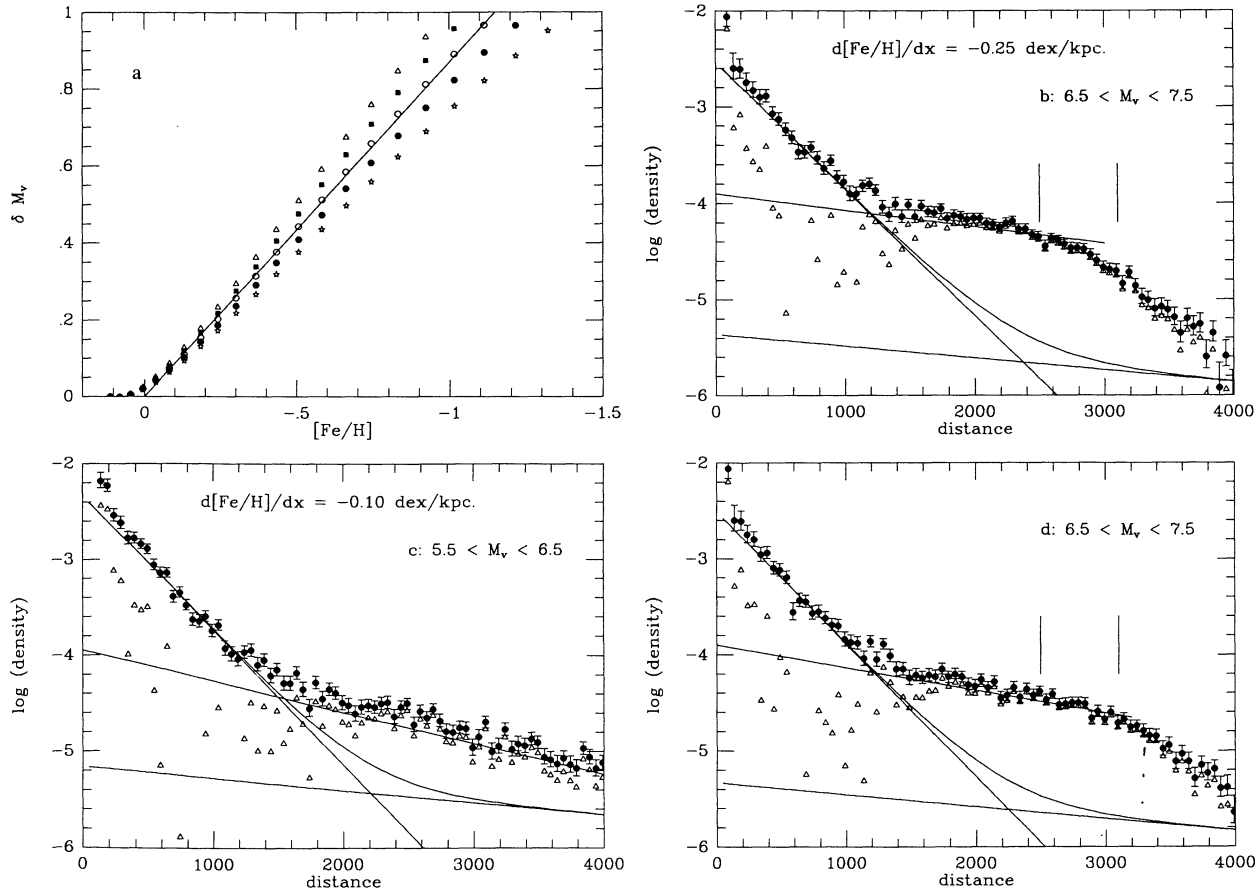

FIG. 11.—(*a*) Relation between decreasing abundance and subluminosity derived from Laird et al.'s (1989) relation between ultraviolet excess and δM_v. The different symbols represent different $(B-V)$ colors from $(B-V) = 0.7$ mag (*triangles*) to 1.1 mag (*stars*). The line plots the approximate relation we have used. (*b*) Density law toward the south Galactic pole if we assume a linear gradient of -0.25 dex kpc^{-1}. The symbols have the same meanings as in Fig. 10. The exponential fitted through the residual densities has a scale height of 2500 pc and a local normalization of $\sim 3\%$ that of the disk. (*c*, *d*) Density laws toward the south Galactic pole derived for an abundance gradient of -0.1 dex kpc^{-1}. Parameters for the exponentials matched to the E/T disk are given in Table 6B.

star $[M_v, (V-I)]$ relation, but Laird et al. (1989) have derived a series of equations between ultraviolet excess, $\delta_{0.6}$, and subluminosity, δM_v, and we have used Carney's (1979) calibration of $\delta_{0.6}$ to calibrate δM_v against abundance. Figure 11*a* plots the results for $(B-V)$ colors between 0.7 and 1.1 mag ($M_v \sim +4.5$ to $+7.5$). Limiting ourselves to [Fe/H] > -1, we can use the simple approximation

$$\delta M_v = -0.87\delta[\mathrm{Fe/H}] .$$

The most important result from these calculations is that the overall morphology is unaltered from the uniform abundance density distributions plotted in Figure 9. The fits to the old disk are, indeed, almost unchanged, but at larger z the lower luminosities for individual stars increase the densities and produce flatter distributions. With the -0.25 dex kpc^{-1} gradient this leads to E/T disk scale heights in excess of 2 kpc, particularly for the fainter stars (Table 6C); the exponential fit plotted in Figure 11*b* is for a 2500 pc scale height and a local normalization of $\sim 3\%$ ρ_0(disk). With these parameters the E/T disk dominates in the blue for $V > 14$, and the model predictions (even with a much reduced local density) are clearly unacceptable (model *i* in Table 4). (Note that in the model, the gradient results from the mixing of the two populations with different scale heights and mean abundances.)

Adopting the smaller abundance gradient, however, gives more consistent results among the different absolute magnitude intervals, although the E/T disk scale heights and density normalizations again are higher for the fainter stars (Table 6B and Figs. 11*c* and 11*d*). As with the no-gradient results (Fig. 9), star-count analysis favors the smaller scale heights and lower density normalizations. Table 4, model *j*, shows that a model with an E/T disk based directly on the analysis of $6.5 < M_v < 8.5$ stars predicts substantially too many blue and intermediate-colored stars at faint magnitudes. Determining whether these discrepancies (between different ranges in M_v) reflect problems in the GR83 data and the calibration methods or inadequacies in the model (particularly the simplistic parameterization of the density distribution) must await higher accuracy data sets. However, our present analysis shows that steeper abundance gradients lead to more discordant results, hence we favor a relatively shallow abundance gradient with height above the plane in the disk.

Given this abundance gradient, which we are modeling as the sum of discrete components, we should reconsider the color-magnitude diagram that is appropriate for the E/T disk. Insofar as a two-component exponential approximation is representative of the density laws of the disk, Figure 3 shows that we are sampling the old disk at $z \sim 700$ pc and the E/T disk at

TABLE 7

MAIN-SEQUENCE COLOR-MAGNITUDE DISTRIBUTIONS

	$(B-V)$		
M_v	Old disk	Mid	47 Tuc
4.....	0.50	0.51	0.51
5.....	0.63	0.59	0.55
6.....	0.83	0.76	0.69
7.....	1.04	0.97	0.90
8.....	1.29	1.21	1.13
9.....	1.46	1.39	1.32
10.....	1.51	1.46	1.41

NOTE.—The $[M_v, (B-V)]$ relations used for the E/T disk in our models. The old disk relation is derived from observations of nearby stars of known trigonometric parallax, and the 47 Tuc observations are taken from Hesser et al. 1987. The "Mid" color-magnitude relation is simply a linear interpolation between these two empirical data sets.

$z \sim 2$–3 kpc (a 1400 pc scale height, rather than 1200 pc, will stretch the distance scale by only $\sim 15\%$). So for an average gradient of ~ -0.1 dex kpc^{-1} we would expect an average abundance of -0.3 to -0.4 dex for the latter stars, rather than the [Fe/H] $= -0.7$ of 47 Tuc. There is mild supporting evidence for this hypothesis in that the 47 Tuc–like E/T disk lies slightly to the blue of the observations at $V = 17$ (Figs. 4*c* and 7*c*). Moreover, a mean abundance of [Fe/H] $= -0.4$ is also consistent with the *UBV* photometry in SRM and with the spectroscopic observations by Friel (1987), Hartkopf & Yoss (1982), and (in two of their three fields) Ratnatunga & Freeman (1989), while Carney et al. (1989) derive [Fe/H] $= -0.5$. For our present purposes we have constructed an intermediate-abundance ([Fe/H] ~ -0.4) color-magnitude diagram midway between the 47 Tuc and nearby-star relations (Table 7). As we shall describe in § 4.3, this provides a reasonable match (for a preliminary model to the observations.

4.2.3. *Summary*

Reviewing the density structure toward the south Galactic cap, we find that the old disk, at least for $M_v < +8$, is well represented by an exponential distribution with an average scale height of ~ 325 pc. This holds whether one assumes no abundance gradient or adopts a gradient as high as -0.25 dex kpc^{-1}. In the latter case, however, subtracting the contribution of the old disk and halo stars leads to a flat distribution of residuals and effective exponential scale heights of 2 kpc or more for the E/T disk. Lesser abundance gradients, based on the SRM ultraviolet excess data, lead to residual densities which can be matched by exponential distributions with scale heights in the range 1350–1800 pc and local density normalizations of 4.0%–2.5% ρ_0(disk). The SA 57 star-count data, however, limit the permissible range to scale heights of ~ 1400–1600 pc and normalizations of 2.5%–2.0% ρ_0(disk). Finally, a less steep abundance gradient implies a mean abundance of [Fe/H] ~ -0.4 for the E/T disk, and to take this into account we have constructed color-magnitude relations intermediate between those of the old disk and 47 Tuc.

4.3. *An Interim Model*

Star-count models have an impressive array of adjustable parameters with the result that it is possible, by judicious tweaking, to match almost any set of observations. This is particularly so, given the scarcity of accurate observational data. Obtaining deep, galaxy-free, multicolor data in other fields is an essential prerequisite to our disentangling the complexities of Galactic structure, and we are currently engaged in such a project. Hence the model that we present here is preliminary, aimed merely at providing a better match to the north Galactic pole data. It is our expectation that future observations will reveal inadequacies in this model just as we have found problems in the current "standard" model.

The main parameters of our interim model are listed as model *k* in Table 4. (To underline the remaining uncertainties, any of models *l*–*n* is a valid alternative.) The model predictions are compared with the north Galactic pole data in Figure 12. For the halo we have adopted the GC luminosity function that we derived in § 4.1.1 and have modeled the spatial distribution as a de Vaucouleurs spheroid, effective radius 2.67 kpc with an axial ratio c/a of 0.8. The observed number counts then require a local halo-to-disk number ratio of $\sim 0.15\%$. Single-component, flatter density distributions require a higher local normalization and predict a shallower gradient in the differential star counts and, as a result, provide a poorer match to the SA 57 data (Table 4, models *d* and *f*). However, as we described in § 4.1.3, this does not preclude the existence of a second substantial component in a separate, significantly flatter distribution; for example, including a subpopulation with c/a of 0.4 and a local halo-to-disk ratio of 0.1% (i.e., encompassing 40% of the nearby subdwarfs) adds only ~ 6–8 halo stars deg^{-2} between $V = 19$ and $V = 20$ (compare models *k* and *m* in Table 4). Hence the star-count data are not inconsistent with a *total* halo-to-disk ratio locally of $\sim 0.25\%$, and an orbital distribution similar to that proposed by SLZ.

Considering the disk, both the color distributions toward the north Galactic pole and the density laws clearly require a significant component in an extended distribution. In neither case are there unique solutions, since one can match the observations by trading off among the local density normalization, the scale height, and the color-magnitude diagram. Figures 12*d* and 12*e* show that the peak of the E/T disk distribution falls at intermediate colors between 18th and 20th magnitudes, and with sufficient data (i.e., covering larger solid angles) it will be possible to set more accurate constraints on some parameters. Deep *I*-band data for the north Galactic pole field will also help to disentangle the density distributions. For present purposes, however, we have adopted a 1400 pc exponential distribution for the E/T disk. The local normalization is 2.5% that of the old disk, and we adopt the intermediate-abundance color-magnitude diagram described in § 4.2.2.

In Figure 12 we have matched our interim model against the north Galactic pole observations; we include plots of the color distributions both fainter than $V = 22$ and brighter than $V = 16$. The only substantial discrepancy in the total number counts lies at the faintest magnitudes, with the model and the data diverging for $V > 20.5$. Figure 12*f* shows that the model underpredicts both the blue and the red peaks. It is likely that most of the problem in matching the bluer objects lies with residual extragalactic contamination; the difference between the interim model and the observations at $20 < V < 21$ is only $\sim 15\%$, compatible with the estimates given in § 2.2. A slightly flatter halo (or a higher local density) gives a better match at $20 < V < 21$ but predicts too many halo stars at brighter magnitudes. Given the number of stars involved, the differences may also reflect the relatively small size of the current sample.

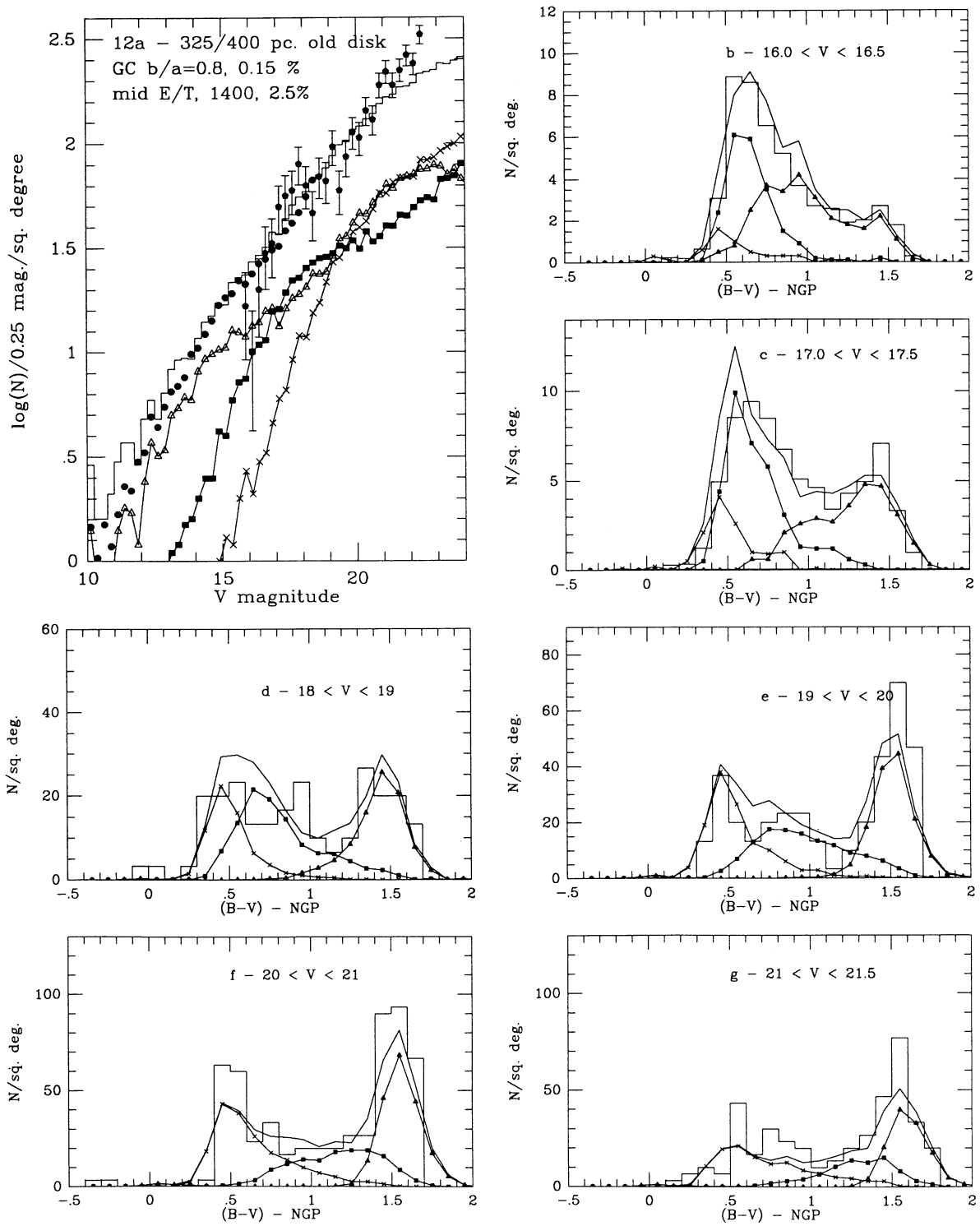

FIG. 12.—Differential star counts, $A(m)$, and color distributions predicted by our interim model discussed in § 4.3. We adopt the GC luminosity function (Fig. 5*e*) for the halo, with an axial ratio (c/a) of 0.8 and a local halo/disk ratio of 0.15%; the E/T disk has a mildly metal-poor ([Fe/H] ~ -0.4] color-magnitude relation, a 1400 pc scale height, and a local density 2.5% that of the disk; and old disk stars with $M_v \geq +9$ have an exponential scale height of 400 pc. The symbols have the same meanings as in Fig. 4. In addition to the magnitude intervals plotted in Figs. 4, 7, and 8, we have compared the model predictions with Kron's data for $22 < V < 22.5$ (panel *h*) and with Stobie & Ishida's (1987) observations of stars brighter than 16th magnitude (panels *i*, *j*, and *k*).

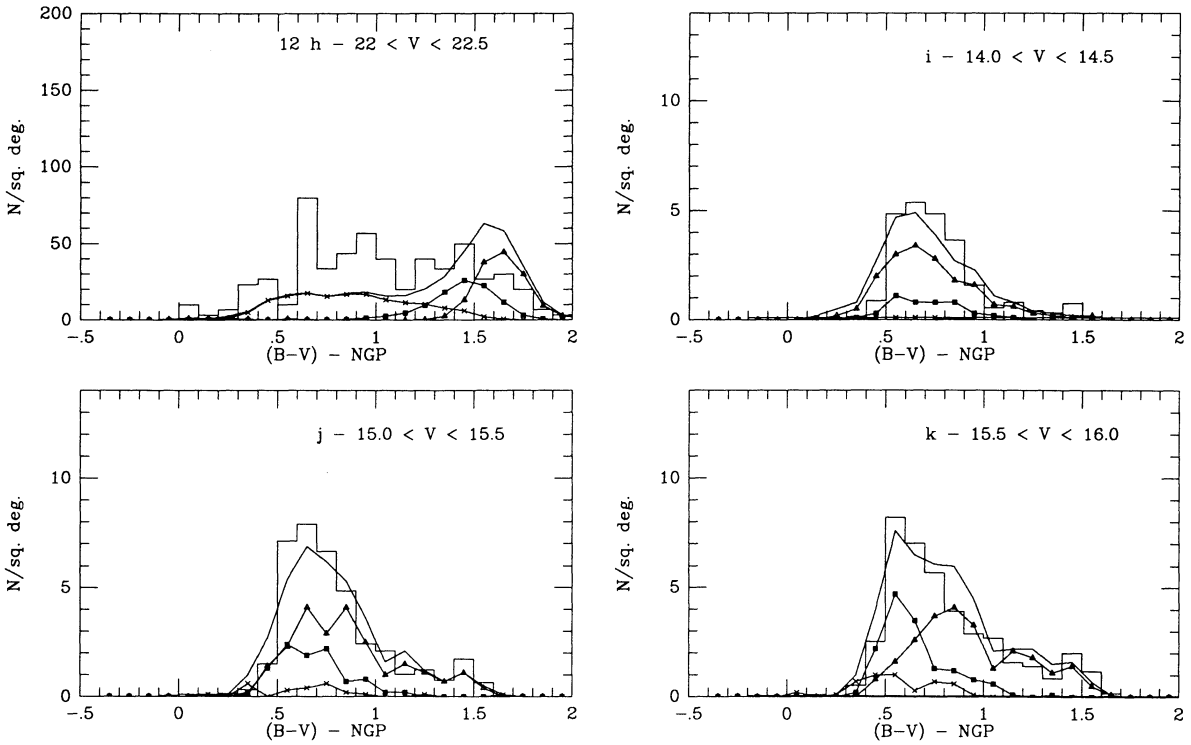

FIG. 12—*Continued*

The data also exceed the model predictions in the red. (We note that Koo et al. 1986 derived a similar conclusion from analysis of their SA 57 data set.) An argument against most of the red objects being extragalactic comes from the proper-motion measurements (SRM). The proper-motion index

$$\mu_i = \left[\left(\frac{\mu_\alpha}{\epsilon_{\mu\alpha}}\right)^2 + \left(\frac{\mu_\delta}{\epsilon_{\mu\delta}}\right)^2\right]^{1/2}$$

measures the statistical significance of a given object's proper motion. More than 50% of the faintest ($21.5 > R_F > 21$) red objects in the sample have 4 σ motions (and at least 75% have 3 σ motions), implying that the majority are indeed Galactic stars. With a redder color-magnitude diagram, the E/T disk contributes to some extent toward fitting the substantial red peaks that are evident in the SA 57 data fainter than 19th magnitude. However, the bulk of the M stars must be from the old disk, and since, the average distance modulus is expected to be ~ 9 (Fig. 3), the relevant stars are expected to have $M_v \sim +9$ or fainter. [The degeneracy of the $(B-V)$ [or $(B_J - R_F)$] color index prevents our being categorical on this point. Once I-band photometry is available for the SA 57 stars, the $(R-I)$ colors will allow a better determination of the absolute magnitude distribution of the red-peak stars.] The options available to rectify this defect are, first, invoking a modified luminosity function (although this requires our *doubling* the local density of stars with $M_v > +9$); second, a flatter density law (that is, in our approximation, a higher scale height); and, third, a combination of the two. The scale heights listed in Table 6 (and plotted in Figure 5 of GR83) offer marginal evidence for an increased scale height for $M_v > +8$, although this may very well simply reflect the difficulty of distinguishing the E/T disk with the smaller distance limits at these fainter absolute magnitudes. In any event, for current purposes we have adopted a scale height of 325 pc for the old disk stars with $M_v \leq +8$, but use 400 pc for the fainter stars. Even this model produces a consistent shortfall in the predicted numbers in the red peak for $V > 19$.

Considering the total star counts, it is possible that misclassified galaxies (cf. Fig. 1) are artificially boosting the counts at the faintest magnitudes ($V > 22$). Figure 12*h* plots the observed and predicted $(B-V)$ distributions for $22 < V < 22.5$ (these data are drawn entirely from Kron's catalog), and it is clear that the excess of observed objects is relatively uniformly distributed in color, although the increased photometric uncertainties near the plate limit obscure much of the structure in this diagram. It remains possible that our assumptions are incorrect concerning either or both the form of the disk luminosity function at faint magnitudes $M_v > +10$ ($V > 19$) and the appropriate density laws for those stars. I-band photometry, and $(R-I)$ colors, for the SA 57 stars will go some way toward settling this issue. Indeed, further progress in improving the accuracy of our model must rest on obtaining more deep, multicolor observations, both expanding the areal coverage toward the Galactic poles and extending the survey to fields at other Galactic orientations.

5. CONCLUSIONS

The main aim of this paper is to demonstrate that significant discrepancies exist between the standard model that is usually adopted to characterize the Galaxy and the observed color distribution at faint magnitudes toward the north Galactic pole. Although the total number counts fainter than $V = 18$ are in relatively good agreement with observations, the contribution of halo [$(B-V) \sim 0.06$] stars is overestimated substan-

tially and the fraction of disk $[(B-V) > 1.3]$ stars correspondingly underestimated. Moreover the *disk* is the dominant population to at least $V = 21$.

We have used star-count models in an initial reinvestigation of this problem, although we would emphasize that, with deep, accurate photometry in only one field, the observational constraints are limited. Our model is no more than a first attempt at a better representation of the Galaxy. However, the current analysis suggests that a major problem affecting past modeling of the halo stems from the use of a luminosity function that is inappropriate to an extremely old population. We have redetermined the halo luminosity function, using data from globular cluster observations, and find that the SA 57 data are well matched by a somewhat flattened $(c/a \sim 0.8 \pm 0.05)$ $r^{1/4}$ halo with a local halo-to-disk ratio of $\sim 0.15\% \pm 0.03\%$. A multicomponent halo, with a significant fraction of the local stars in flatter components, is also a possibility.

We have modeled the disk populations of the Galaxy as the sum of several exponential density distributions. We find that the extended/thick disk subpopulation can be represented adequately if we adopt scale heights in the range 1400–1600 pc and corresponding normalizations (relative to the local disk density) of ~2.5–2.0. These values are closer to those originally proposed by GR83 than the smaller scale heights which have been cited more recently. Moreover, the north Galactic pole observations suggest that the color-magnitude diagram (at least at $z \sim 3$ kpc) is closer to that of the old disk than the metal-rich ([Fe/H] ~ -0.65) globular 47 Tuc. As to the old disk, the strong peak at $(B-V) \sim 1.5$ in the SA 57 color-magnitude diagram between 18th and 21st visual magnitude appears to require a scale height of 400 pc for the faintest stars $(M_v > +9)$ in the old disk. We should underline the point that while we have used separate exponential functions to represent the disk components, there is no compelling reason to hold that these are either separate populations or that they follow this functional form exactly.

The interim model that we have presented here provides a better match to the observed data but is still no more than loosely constrained by observations. Within SA 57 itself, we require longer wavelength (specifically *I*-band) observations of the red stars with $V > 20$ to determine absolute magnitudes and separate old disk and E/T disk stars; we require more accurate photometry (and removal of extragalactic contaminants) for the fainter ($V > 21.5$) stars; and we require coverage of a larger solid angle to obtain a more accurate estimate of the disk density laws. Finally, we require similar data at other Galactic latitudes in order that we may set better limits on the axial ratio (or the range of axial ratios) in the halo, on the scale length of the Galactic disk, and on the range of abundance at heights of 2–5 kpc above the Galactic plane. Such data can now be obtained using large-format CCD detectors on relatively small telescopes, and we intend that this be the first of a series of papers using both these techniques and deep photographic photometry to address these important questions.

We thank Heather Morrison, Bruce Carney, Mario Mateo, and George Preston for helpful comments.

REFERENCES

Armandroff, T. 1989, AJ, 97, 375
Arnold, R. 1990, MNRAS, 244, 465
Arp, H. C., & Hartwick, F. D. A. 1971, ApJ, 167, 499
Bahcall, J. N. 1986, ARA&A, 24, 577
Bahcall, J. N., & Casertano, S. 1986, ApJ, 308, 347
Bahcall, J. N., Ratnatunga, K. U., Buser, R., Fenkart, R. P., & Spaenhauer, A. 1985, ApJ, 299, 616
Bahcall, J. N., & Soneira, R. M. 1980, ApJS, 44, 73 (BS80)
———. 1984, ApJS, 55, 67 (BS84)
Becker, W., Fang, Ch., Fenkart, R. P., Hassam, S. M., Karaali, S., Marsoglu, A., Spaenhauer, A., & Topaktas, L. 1983, Publ. Astron. Inst. Basel, Vol. 9
Becker, W., & Fenkart, R. 1976, Photometric Catalogue of Stars in Selected Areas and Other Fields in the RGU-System (Basel: Astron. Inst. Univ. Basel), Vol. 1
Bergbusch, P. A. 1990, AJ, 100, 182
Bergbusch, P. A., & VandenBerg, D. 1992, ApJS, 81, 163
Bessell, M. S. 1990, A&AS, 83, 357
Blaauw, A. 1960, MNRAS, 121, 164
Burstein, D., & Heiles, C. 1982, AJ, 87, 1165
Buser, R., & Kaeser, U. 1985, A&A, 145, 1
Camm, G. L. 1950, MNRAS, 110, 305
Carney, B. W. 1979, ApJ, 233, 211
Carney, B. W., Aguilar, L., Latham, D. W., & Laird, J. B. 1990a, AJ, 99, 201
Carney, B. W., & Latham, D. W. 1986, AJ, 92, 60
Carney, B. W., Latham, D. W., & Laird, J. B. 1989, AJ, 97, 423
———. 1990b, AJ, 99, 572
Casertano, S., Ratnatunga, K., & Bahcall, J. N. 1990, ApJ, 357, 435
Chiu, L.-T. G. 1980, ApJS, 44, 31
Cudworth, K., Schweizer, F., & Majewski, S. R. 1993, in preparation
Da Costa, G., Mould, J. R., & Ortolani, S. 1984, ApJ, 282, 125
Dawson, P. C. 1986, ApJ, 311, 984
del Rio, G., & Fenkart, R. 1987, A&AS, 68, 397
de Vaucouleurs, G. 1977, AJ, 82, 456
Djorgovskii, S., & Sosin, C. 1989, ApJ, 341, L13
Elvius, T. 1965, in Stars and Stellar Systems, Vol. 5, Galactic Structure, ed. A. Blauuw & M. Schmidt (Chicago: Univ. Chicago Press), chap. 3
Fahlman, G. G., Richer, H. B., & Nemec, J. 1991, ApJ, 380, 124
Fenkart, R. 1966, Z. Astrophys., 66, 390
Friel, E. D. 1987, AJ, 93, 1388
———. 1988, AJ, 95, 1727
Fukuoka, T., & Simoda, M. 1976, PASJ, 28, 633
Gilmore, G. F. 1981, MNRAS, 195, 183
———. 1984, MNRAS, 207, 223
Gilmore, G. F., & Reid, I. N. 1983, MNRAS, 202, 1025 (GR83)
Gilmore, G. F., Reid, I. N., & Hewett, P. C. 1985, MNRAS, 213, 257
Gilmore, G. F., & Wyse, R. G. 1985, AJ, 90, 2015
Gilmore, G. F., Wyse, R. G., & Kuijken, K. 1989, ARA&A, 27, 555
Gliese, W. 1969, Veröff. Astron. Rechen-Inst. Heidelberg, No. 22
Green, E. M., Demarque, P., & King, C. R. 1987, The Revised Yale Isochrones and Luminosity Functions (New Haven: Yale Univ. Obs.)
Green, E. M., & Morrison, H. 1992, in ASP Conf. Ser., Vol. 42, The Globular Cluster–Galaxy Connection, ed. G. H. Smith & J. P. Brodie (San Francisco: ASP)
Harris, W. 1976, AJ, 81, 1095
Hartkopf, W. I., & Yoss, K. M. 1982, AJ, 87, 1679
Hartwick, F. D. A. 1970, ApJ, 161, 845
———. 1983, Mem. Soc. Astron. Italiana, 54, 51
———. 1987, in NATO A.S.I., The Galaxy, ed. G. Gilmore & R. Carswell (Dordrecht: Kluwer), 281
Hawkins, M. R. S. 1984, MNRAS, 206, 433
Herschel, W. 1785, Phil. Trans., 75, 213
Hesser, J. E., Harris, W. E., VandenBerg, D., Allwright, J. W. B., Shott, P., & Stetson, P. B. 1987, PASP, 99, 739
Hurley, D. J. C., Richer, H. B., & Fahlman, G. G. 1989, AJ, 98, 2124
Kapteyn, J. C. 1922, ApJ, 55, 302
King, C. R., Da Costa, G. S., & Demarque, P. 1985, ApJ, 299, 674
Kinman, T. D. 1965, ApJS, 11, 199
———. 1992, in ASP Conf. Ser., Vol. 30, Variable Stars and Galaxies, ed. B. Warner (San Francisco: ASP), 19
Kinman, T. D., Wirtanen, C. A., & Janes, J. A. 1966, ApJS, 13, 379
Koo, D. C., Kron, R. G., & Cudworth, K. 1986, PASP, 98, 599
Kraft, R. P. 1989, PASP, 101, 1113
Kraft, R. P., Sneden, C., Langer, G. E., & Prosser, C. F. 1992, AJ, 104, 645
Kron, R. G. 1980, ApJS, 43, 305
Kron, R. G., Bershady, M. A., Munn, J. A., Smetanka, J. J., Majewski, S., & Koo, D. C. 1991, in ASP Conf. Ser., Vol. 21, The Space Distribution of Quasars, ed. D. Crampton (Provo: ASP), 32
Kroupa, P., Tout, C. A., & Gilmore, G. F. 1991, MNRAS, 251, 293
———. 1993, MNRAS, in press
Kuijken, K., & Gilmore, G. 1989, MNRAS, 239, 605
Laird, J. B., Carney, B. W., & Latham, D. W. 1989, AJ, 95, 1843
Laird, J. B., Rupen, M. P., Carney, B. W., & Latham, D. W. 1988, AJ, 96, 1908
Layden, A. 1992, in ASP Conf. Ser., Vol. 42, The Globular Cluster–Galaxy Connection, ed. G. H. Smith & J. P. Brodie (San Francisco: ASP)
Leggett, S. K. 1992, ApJS, 82, 351
Levison, H. F., & Richstone, D. O. 1986, ApJ, 308, 623

Luyten, W. J. 1976, The Half-Second Catalogue (Minneapolis: Minnesota Univ.)
Magnani, L., Blitz, L., & Mundy, L. 1985, ApJ, 295, 402
Majewski, S. R. 1991, in Precision Photometry, ed. A. G. Davis Philip, A. R. Upgren, & K. Janes (Schenectady: Davis), 209
———. 1992, ApJS, 78, 76 (SRM)
Majewski, S. R., Munn, J. A., Kron, R. G., Bershady, M. A., Smetanka, J. J., & Koo, D. C. 1991, in ASP Conf. Ser., Vol. 21, The Space Distribution of Quasars, ed. D. Crampton (Provo: ASP), 55
McClure, R. D., & Twarog, B. A. 1977, ApJ, 214, 111
McClure, R. D., VandenBerg, D., Bell, R. A., Hesser, J. E., & Stetson, P. B. 1987, AJ, 93, 1144
Miller, G. E., & Scalo, J. M. 1979, ApJS, 41, 513
Morrison, H. L. 1992, preprint
Morrison, H. L., Flynn, C., & Freeman, K. C. 1990, AJ, 100, 1191
Murray, C. A. 1986, MNRAS, 223, 649
Norris, J. E. 1986, ApJS, 61, 667
———. 1987a, ApJ, 314, L39
———. 1987b, AJ, 93, 616
Norris, J., & Green, E. M. 1989, ApJ, 337, 272
Norris, J., & Ryan, S. G. 1991, ApJ, 380, 403
Oort, J. H. 1932, Bull. Astr. Inst. Netherlands, 6 (No. 238)
———. 1958, Ric. Astron., 5, 415
Oort, J. H., & Plaut, L. 1975, A&A, 41, 71
Paez, E., Straniero, O., & Martinez Roger, C. 1990, A&AS, 84, 481
Piotto, G., Cappacioli, M., Ortolani, S., Rosino, L., Alcaino, G., & Liller, W. 1987, AJ, 94, 360
Preston, G. W. 1957, ApJ, 130, 507
Preston, G. W., Shectman, S. A., & Beers, T. C. 1991, ApJ, 375, 121
Ratnatunga, K., & Freeman, K. C. 1989, ApJ, 339, 126
Reid, I. N. 1984, MNRAS, 206, 1
———. 1987, MNRAS, 225, 873
———. 1990, MNRAS, 247, 70
———. 1991, AJ, 102, 1428
———. 1993, ASP Conf. Ser., Vol. 39, in Galaxy Evolution: The Milky Way Perspective, ed. S. R. Majewski (ASP: Provo), in press
Reid, I. N., & Gilmore, G. F. 1982, MNRAS, 201, 77
Richer, H. B., & Fahlman, G. G. 1992, Nature, 358, 383
Richer, H. B., Fahlman, G. G., Buonanno, R., Fusi Pecci, F., Searle, L., & Thompson, I. 1991, ApJ, 381, 147
Richstone, D. O., & Graham, F. G. 1981, ApJ, 248, 516
Robin, A., & Crézé, M. 1986a, A&A, 157, 1
———. 1986b, A&AS, 64, 53
Rose, J. A. 1985, AJ, 90, 787
Rose, J. A., & Agostino, R. 1991, AJ, 101, 950
Ryan, S., & Norris, J. E. 1991, AJ, 101, 1865
Saha, A. 1985, ApJ, 289, 310
Saio, H., & Yoshii, Y. 1979, PASP, 91, 553
Sandage, A. 1957, ApJ, 125, 422
Sandage, A. 1987, AJ, 93, 610
Sandage, A., & Fouts, G. 1987, AJ, 93, 74
Sandage, A., & Katem, B. 1983, AJ, 88, 1146
Sato, T., Richer, H. B., & Fahlman, G. G. 1989, AJ, 98, 1335
Schmidt, M. 1959, ApJ, 129, 243
———. 1962, ApJ, 137, 243
———. 1975, ApJ, 202, 22
Smith, G. H., McClure, R. D., Stetson, P. B., Hesser, J. E., & Bolte, M. 1986, AJ, 91, 842
Sommer-Larsen, J. 1986, Licentiate thesis, Copenhagen Univ.
Sommer-Larsen, J., & Zhen, C. 1990, MNRAS, 242, 10 (SLZ)
Spaenhauer, A. 1989, Van Vleck Obs. Publ., 9, 45
Stetson, P. B. 1979, AJ, 84, 1056
Stetson, P. B., & Harris, W. E. 1988, AJ, 96, 909
Stobie, R. S., & Ishida, K. 1987, AJ, 93, 624
Stobie, R. S., Ishida, K., & Peacock, J. A. 1989, MNRAS, 238, 709 (SIP89)
Strugnell, P., Reid, I. N., & Murray, C. A. 1987, MNRAS, 220, 413
Suntzeff, N. 1981, ApJS, 47, 1
Suntzeff, N. B., Kinman, T., & Kraft, R. P. 1991, ApJ, 367, 528
Tayler, R. J. 1954, AJ, 59, 413
Tinney, C. G., Mould, J. R., & Reid, I. N. 1992, ApJ, 396, 173
Toller, G. N. 1981, Ph.D. thesis, State Univ. NY Stony Brook
Trevese, D., Kron, R. G., Koo, D. C., & Majewski, S. R. 1993, ApJ, submitted
Upgren, A. R., Weis, E. W., & Hanson, R. B. 1985, AJ, 90, 2039
VandenBerg, D., & Bell, R. A. 1985, ApJS, 58, 561
van den Bergh, S. 1975, ApJ, 201, 585
van der Kruit, P. C., & Searle, L. 1982, A&A, 110, 61
van der Marel, R. P. 1991, MNRAS, 248, 515
von Hippel, T., & Bothun, G. D. 1992, Cambridge preprint
von Seeliger, H. 1898, Abh. K. Bayer. Akad. Wiss., Ser. II, Kl. 19, 564
Wesselink, T. 1987, A Photometric Study of Variable Stars in a Field near the Galactic Centre (Nijmegen: Braldsenstein)
White, S. D. M. 1985, ApJ, 294, L99
Wielen, R. 1974, in Highlights Astron., ed. G. Contopolous (Dordrecht: Reidel), 3, 395
Wielen, R., & Fuchs, B. 1983, in IAU Symp. 106, The Milky Way Galaxy, ed. H. van Woerden, R. J. Allen, & W. B. Burton (Dordrecht: Reidel), 481
Wielen, R., Jahreiss, H., & Kruger, R. 1983, in IAU Colloq. 76, The Nearby Stars and the Luminosity Function, ed. A. G. Davis Philip & A. R. Upgren (Schenectady: Davis), 163 (WJK)
Woolley, R. v.d.r. 1978, MNRAS, 184, 311
Wyse, R. F. G., & Gilmore, G. F. 1989, Comm. Astrophys., 13, 135
Yamagata, T., & Yoshii, Y. 1992, AJ, 103, 117
Yoshii, Y., Ishida, K., & Stobie, R. S. 1987, AJ, 93, 323
Yoss, K. M., Neese, C. L., & Hartkopf, W. I. 1987, AJ, 94, 1600
Zinn, R. 1985, ApJ, 293, 424
Zinn, R., & West, M. 1984, ApJS, 55, 45